iScience

CellPress
OPEN ACCESS

Article

ApoE maintains neuronal integrity via microRNA and H3K27me3-mediated repression

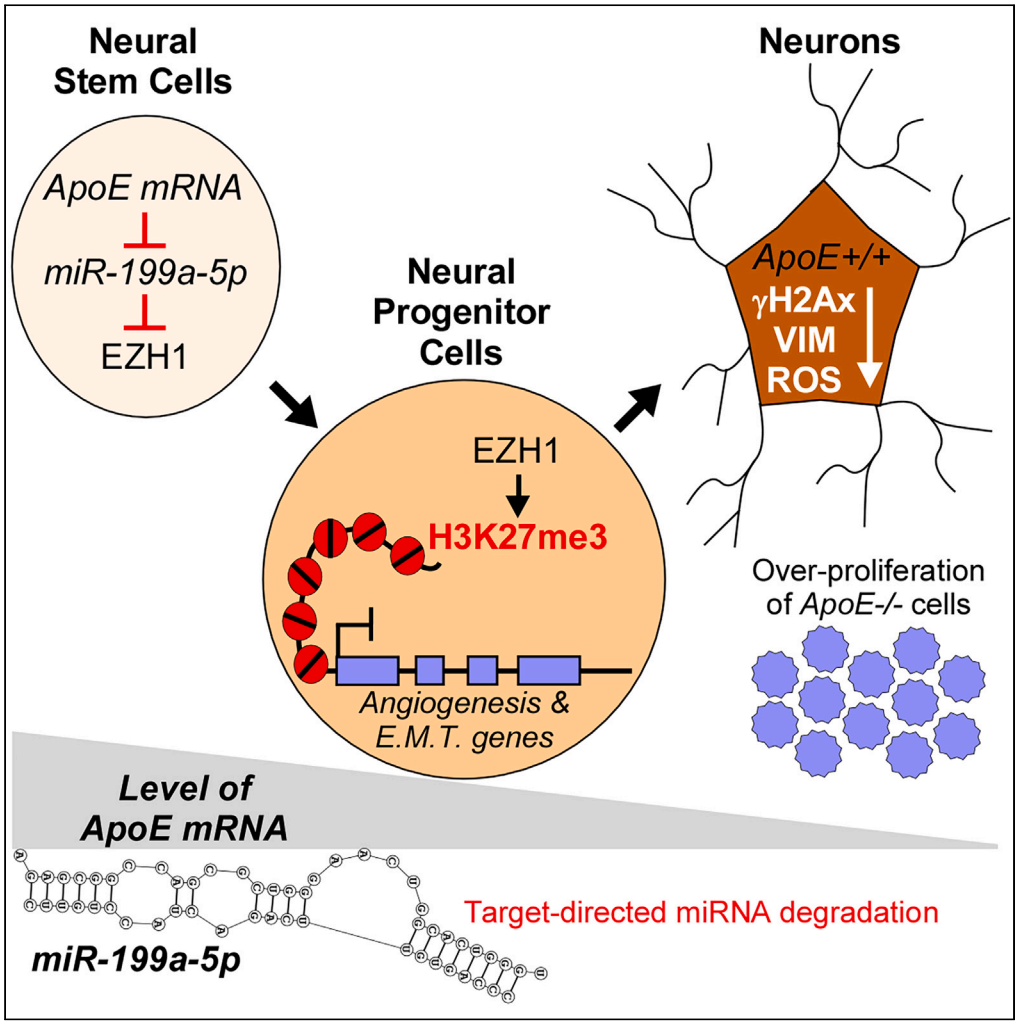

Jiazi Tan, Yow-Yong Tan, Zhen-Kai Ngian, ..., Jiong-Wei Wang, Xianmin Zeng, Chin-Tong Ong

chintong@tll.org.sg

Highlights

Transcriptome of neurons induced *in vitro* resembled their midbrain counterparts

ApoE mRNA silences *miR-199a-5p* in human NSC by target-directed miRNA degradation

miR-199a-5p represses EZH1 in *ApoE* deficient human NSC and NPC during neurogenesis

Repression of non-neuronal genes by H3K27me3 ensures the integrity of mature neurons

Tan et al., iScience *27*, 109231
March 15, 2024
https://doi.org/10.1016/j.isci.2024.109231

iScience

CellPress
OPEN ACCESS

Article

ApoE maintains neuronal integrity via microRNA and H3K27me3-mediated repression

Jiazi Tan,[1] Yow-Yong Tan,[1,2] Zhen-Kai Ngian,[1] Suet-Yen Chong,[3,4] Vinay Kumar Rao,[1,5] Jiong-Wei Wang,[3,4,6,7] Xianmin Zeng,[7,8] and Chin-Tong Ong[1,2,9,*]

SUMMARY

ApoE regulates neurogenesis, although how it influences genetic programs remains elusive. Cortical neurons induced from isogenic control and *ApoE−/−* human neural stem cells (NSCs) recapitulated key transcriptomic signatures of *in vivo* counterparts identified from single-cell human midbrain. Surprisingly, ApoE expression in NSC and neural progenitor cells (NPCs) is not required for differentiation. Instead, ApoE prevents the over-proliferation of non-neuronal cells during extended neuronal culture when it is not expressed. Elevated *miR-199a-5p* level in *ApoE−/−* cells lowers the EZH1 protein and the repressive H3K27me3 mark, a phenotype rescued by *miR-199a-5p* steric inhibitor. Reduced H3K27me3 at genes linked to extracellular matrix organization and angiogenesis in *ApoE−/−* NPC correlates with their aberrant expression and phenotypes in neurons. Interestingly, the *ApoE* coding sequence, which contains many predicted *miR-199a-5p* binding sites, can repress *miR-199a-5p* without translating into protein. This suggests that *ApoE* maintains neurons integrity through the target-directed miRNA degradation of *miR-199a-5p*, imparting the H3K27me3-mediated repression of non-neuronal genes during differentiation.

INTRODUCTION

ApoE is a glycoprotein that mediates lipoprotein trafficking and peripheral cholesterol metabolism.[1,2] Although predominantly expressed by astrocytes, with a lesser extent in physiologically stressed neurons, ApoE plays crucial roles in regulating different aspects of neurogenesis.[3] Immunoelectron microscopy of human temporal lobes revealed a weak punctate ApoE signal within the cell body and proximal dendrites of cortical neurons, in contrast to its strong immunoreactivity in the astrocytes.[4] This observation led to the suggestion that the uptake of astrocytes secreted ApoE by cortical neurons might be required for regulating neuronal metabolism.[4] Indeed, recent study showed that astrocytic ApoE vectors microRNA (miRNA) species into mouse primary neurons to reprogram cholesterol metabolism and H3K27ac deposition at neuronal genes.[5] ApoE also facilitates the maintenance of the neural progenitor pool in the postnatal dentate gyrus[6] and biases differentiation toward hippocampal neurons instead of astrocytes.[7] It promotes the complexity of dendritic arborization and the spine density of hippocampal neurons,[8] facilitating their repair after closed head injury.[9] Consistent with its potential protective and regenerative roles, an elevated level of ApoE was observed in neurons around the ischemic foci of autopsied human brains with cerebral infarction.[10]

Polymorphism in the *ApoE* gene is the major genetic determinant of late-onset Alzheimer's disease (AD), which is clinically manifested by the toxic accumulation of amyloid-β plaques and neurofibrillary Tau tangles.[11] While *ApoE2* confers protection and *ApoE3* is the common allele among the human population, homozygous *ApoE4* increases the AD risk by 12–15 times.[11] Experiments with transgenic mice expressing different *ApoE* alleles have provided valuable insights into their roles in AD pathogenesis. Neuron-specific ApoE4 expression is associated with increased Tau phosphorylation in the brains[12] and exacerbates Tau-mediated neurodegeneration in a mouse model of tauopathy.[13] ApoE4 also impairs neuronal insulin signaling and insulin-stimulated mitochondrial respiration by trapping insulin receptor in the endosomes.[14] Furthermore, astrocytic ApoE4 can accelerate the early seeding of amyloid pathology and neuritic dystrophy in transgenic mice.[15]

[1]Temasek Life Sciences Laboratory, National University of Singapore, Singapore 117604, Singapore
[2]Department of Biological Sciences, National University of Singapore, Singapore 117543, Singapore
[3]Department of Surgery, Yong Loo Lin School of Medicine, National University of Singapore, Singapore 119228, Singapore
[4]Cardiovascular Research Institute, Yong Loo Lin School of Medicine, National University of Singapore, Singapore 117599, Singapore
[5]Department of Medical Genetics, JSS Medical College, JSS Academy of Higher Education and Research, Mysore 570015, India
[6]Nanomedicine Translational Research Programme, Centre for NanoMedicine, Yong Loo Lin School of Medicine, National University of Singapore, Singapore 117609, Singapore
[7]Department of Physiology, Yong Loo Lin School of Medicine, National University of Singapore, Singapore 117593, Singapore
[8]RxCell Inc, Novato, CA 94945, USA
[9]Lead contact
*Correspondence: chintong@tll.org.sg
https://doi.org/10.1016/j.isci.2024.109231

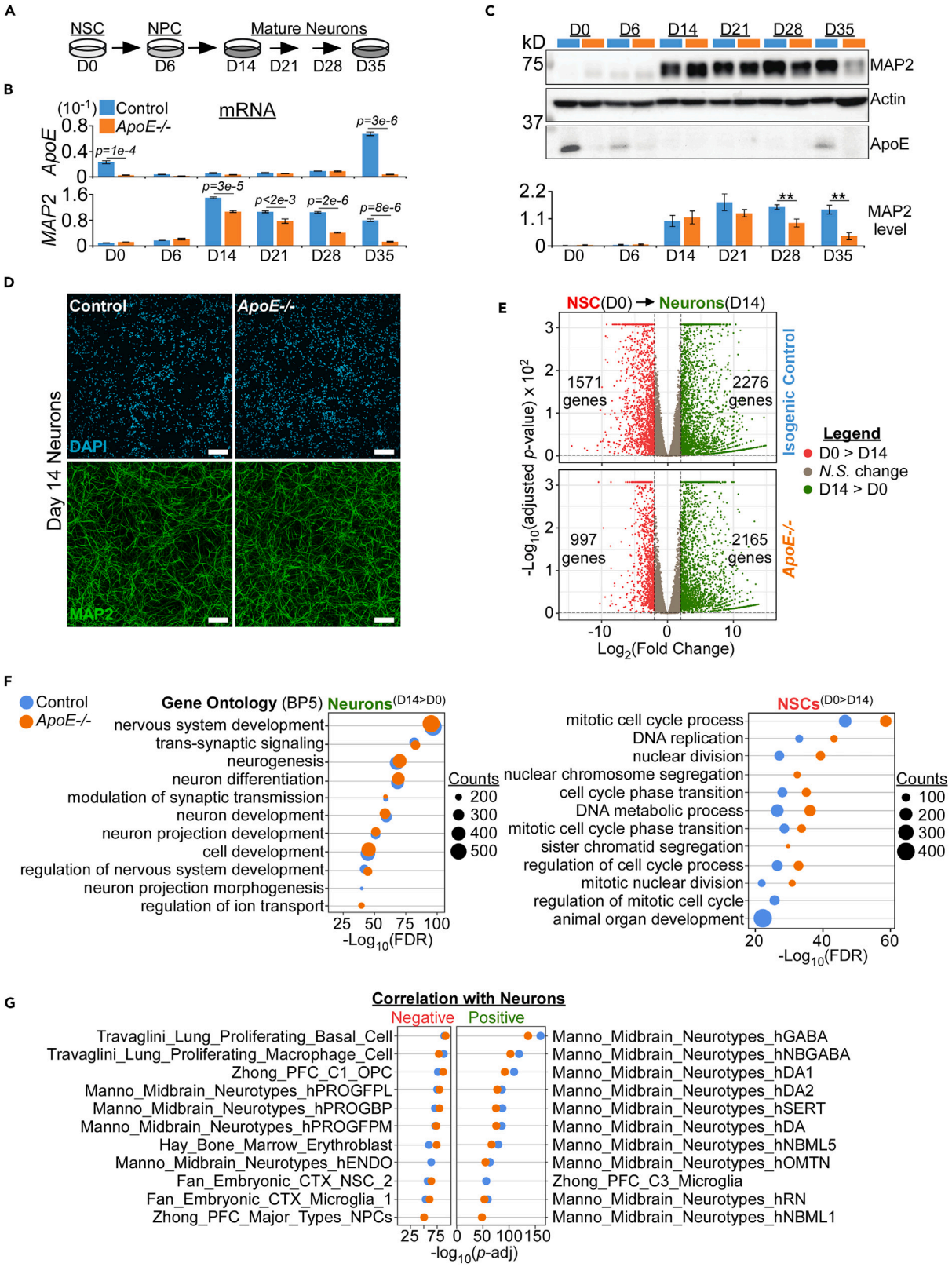
A
NSC
NPC
Mature Neurons
D0
D6
D14
D21
D28
D35
B
mRNA
Control
ApoE-/-
ApoE
MAP2
p=1e-4
p=3e-5
p<2e-3
p=2e-6
p=8e-6
p=3e-6
C
kD
75
37
MAP2
Actin
ApoE
MAP2 level
D
Control
ApoE-/-
Day 14 Neurons
DAPI
MAP2
E
NSC(D0) → Neurons(D14)
1571 genes
2276 genes
997 genes
2165 genes
Isogenic Control
ApoE-/-
Legend
D0 > D14
N.S. change
D14 > D0
-Log10(adjusted p-value) x 10²
Log2(Fold Change)
F
Gene Ontology (BP5)
Neurons(D14>D0)
nervous system development
trans-synaptic signaling
neurogenesis
neuron differentiation
modulation of synaptic transmission
neuron development
neuron projection development
cell development
regulation of nervous system development
neuron projection morphogenesis
regulation of ion transport
Counts
-Log10(FDR)
NSCs(D0>D14)
mitotic cell cycle process
DNA replication
nuclear division
nuclear chromosome segregation
cell cycle phase transition
DNA metabolic process
mitotic cell cycle phase transition
sister chromatid segregation
regulation of cell cycle process
mitotic nuclear division
regulation of mitotic cell cycle
animal organ development
G
Correlation with Neurons
Negative
Positive
Travaglini_Lung_Proliferating_Basal_Cell
Travaglini_Lung_Proliferating_Macrophage_Cell
Zhong_PFC_C1_OPC
Manno_Midbrain_Neurotypes_hPROGFPL
Manno_Midbrain_Neurotypes_hPROGBP
Manno_Midbrain_Neurotypes_hPROGFPM
Hay_Bone_Marrow_Erythroblast
Manno_Midbrain_Neurotypes_hENDO
Fan_Embryonic_CTX_NSC_2
Fan_Embryonic_CTX_Microglia_1
Zhong_PFC_Major_Types_NPCs
Manno_Midbrain_Neurotypes_hGABA
Manno_Midbrain_Neurotypes_hNBGABA
Manno_Midbrain_Neurotypes_hDA1
Manno_Midbrain_Neurotypes_hDA2
Manno_Midbrain_Neurotypes_hSERT
Manno_Midbrain_Neurotypes_hDA
Manno_Midbrain_Neurotypes_hNBML5
Manno_Midbrain_Neurotypes_hOMTN
Zhong_PFC_C3_Microglia
Manno_Midbrain_Neurotypes_hRN
Manno_Midbrain_Neurotypes_hNBML1
-log10(p-adj)

Figure 1. *In vitro* differentiated neurons recapitulate key transcriptional signatures of neurotypes identified from single-cell RNA-sequencing of human ventral midbrain

(A) Differentiation of neuronal stem cells (NSCs) into neural progenitor cells (NPCs) and mature neurons (Day 14), followed by 3 additional weeks of culture. Cells were harvested on different day "D" for experiment.

(B) Measurement of *ApoE* and *MAP2* mRNA level by quantitative PCR (qPCR) in isogenic control and *ApoE−/−* cells harvested on different day. Data are presented as mean ± S.D. (triplicate qPCR reactions, 2-tailed *t*-tests).

(C) Representative immunoblots and MAP2 quantification of cells harvested on different days. Lysates were probed with MAP2, actin and ApoE antibodies. The level of MAP2 was normalized to actin and quantified with reference to Day 14 control neurons. Data presented as mean ± S.E.M (**p < 0.005, n = 5. 2-tailed paired *t*-test).

(D) Representative immmunofluorescence images of Day 14 neurons stained with MAP2 and DAPI. The scale bars represent 150 μm.

(E) RNA-seq volcano plots of differentially expressed genes between NSC and Day 14 neurons as determined by DESeq2 with Log_2(2-fold change) threshold and adjusted p-value <0.05.

(F) Top 10 enriched gene ontology terms (BP: Biological Process) for genes highly expressed in either control or *ApoE−/−* neurons (left) and NSC (right).

(G) Ranked enrichment analysis of gene expression signatures in control and *ApoE−/−* cells (Negative: NSC; Positive: Neurons) by directional *fgsea* statistical enrichment test using cell type signature gene sets. "h" indicates human; GABA: GABAergic neurons; CTX: cerebral cortex; DA: dopaminergic neurons; SERT: serotonergic; NB: neuroblast; NbML: mediolateral neuroblasts; OMTN: oculomotor and trochlear nucleus; RN: red nucleus; OPC: oligodendrocyte precursor cells; PROG: Progenitor; FPL: lateral floorplate; BP: basal plate; FPM: medial floorplate; ENDO: endothelial cells; PFC: prefrontal cortex.

Consistent with clinical and mouse data, ApoE4 also triggers pathological phenotypes in primary neurons or organoids that were derived from human pluripotent stem cells. Induced human GABAergic neurons that expressed ApoE4 have higher levels of Tau phosphorylation and amyloid-β production, which contribute to their degeneration.[16] Consequently, ApoE4 exacerbates synaptic loss and Tau pathology in cerebral organoids derived from patients with AD.[17] ApoE4 also enhances early neuronal differentiation and maturation of neurons;[18] specifically activates cAMP-response element-binding protein (CREB) in rat primary hippocampal neurons[19] and functions as a transcriptional repressor in human neuroblastoma and glioblastoma cells.[20] On the other hand, ApoE3 activates the p44/42 mitogen-activated protein kinase (MAPK) cascade for neurite outgrowth[21] and the extracellular signal-regulated kinase (ERK) pathway for NSC survival[22] but inhibits the c-Jun N-terminal kinase (JNK1/2) pathway in primary mouse cortical neurons.[23]

Interestingly, studies with human cortical neurons induced by neurogenin2 (Ngn-2)[24] showed that different ApoE isoforms stimulate differential transcriptional programs, including the expression level of the amyloid precursor protein gene.[18,25] While these results highlighted the physiological and pathological roles of ApoE3 and Apo4 respectively, they did not address the possible effects caused by *ApoE* deletion as well as mechanism(s) by which ApoE may regulate genetic programs during the differentiation of cortical neurons. We sought to understand the potential cell-autonomous role of ApoE in regulating gene expression in cortical neurons induced by a 14-day neuronal differentiation protocol.[26] The gene expression patterns of these cortical neurons matched the profiles of those generated by Ngn-2 induction (Table S1)[24] and recapitulated the transcriptional signature of their *in vivo* counterparts.[27] Functional analysis uncovered an unexpected epigenetic link between ApoE and *miR-199a-5p* that is necessary for imparting the H3K27me3-mediated repression of non-neuronal genes and maintaining the integrity of differentiated mature cortical neurons.

RESULTS

Transcriptome of *in vitro* differentiated neurons resembles *in vivo* neuronal subtypes

To investigate the role of ApoE in regulating differentiation and the maintenance of neurons, isogenic control (*ApoE3/E4*) and *ApoE−/−* human NSC (Day 0) were induced into NPC (Day 6) and cortical neurons (Day 14), followed by three additional weeks of culture (Figure 1A).[26] The expression levels of ApoE and the neuronal marker Microtubule-Associated Protein 2 (MAP2) were assayed by quantitative PCR (qPCR) and immunoblot. *ApoE* mRNA was expressed and translated into protein in the control NSC and Day 35 neurons (Figures 1B, S1A, and S1B), with a residual level of ApoE protein (relative to NSC) detected at the NPC stage but not at other time-points (Figures 1C and S1C). Consistent with previous studies,[26,28,29] *MAP2* mRNA was detected in the differentiated neurons at Day 14, albeit at a significantly lower in *ApoE−/−* cells (Figures 1B and S1A). On the other hand, the difference in the level of MAP2 protein only became apparent in Day 28 and 35 neurons (Figures 1C and S1D). Similar cellular morphology was observed after the immunostaining of Day 14 neurons with the MAP2 antibody, indicating that ApoE is not necessary for the *in vitro* differentiation of NSC (Figures 1D and S1E). However, the reducing level of MAP2 protein after extended culture of *ApoE−/−* neurons suggests that ApoE may be required for the maintenance of differentiated neurons despite the absence of its mRNA and protein in the neurons before Day 35.

To better understand the genetic programs involved in the differentiation and characterize the cortical neurons, we performed RNA-sequencing of control and *ApoE−/−* cells at Day 0 (NSC), Day 14 and Day 35 (neurons). Differential gene expression patterns between three time-points were determined by DESeq2 using a stringent cut-off with base-mean >100, log_2|fold change| > 2 and adjusted p < 0.05 (Figure 1E; Table S1). Gene ontology (GO) analysis revealed that genes highly expressed in Day 14 neurons as compared to Day 0 NSC were enriched for different neuronal developmental processes (Figure 1F; Table S2). On the other hand, genes with elevated expression in NSC are involved in cell division and DNA replication, consistent with their proliferative characteristics (Figure 1F). Consistent with MAP2 staining patterns, control and *ApoE−/−* Day 14 neurons exhibited highly similar GO terms, indicating that ApoE is not required for neuronal differentiation. Gene set enrichment analysis (GSEA) using cell type signature gene sets from the Molecular Signatures Database (MSigDB)[30,31] revealed that genes highly expressed in Day 14 neurons were positively correlated with the signatures of different neuronal

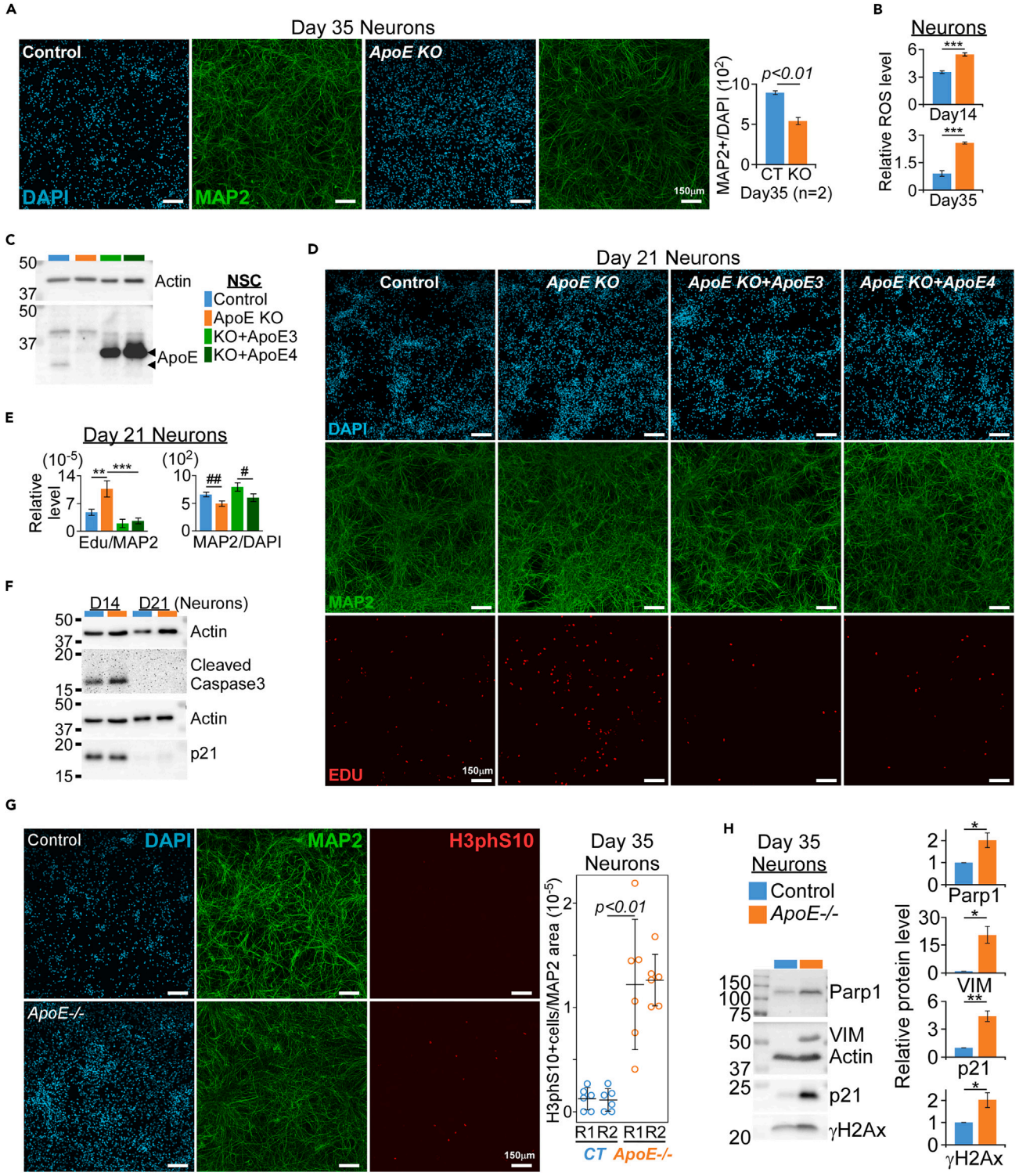

Figure 2. *ApoEε3* and *ε4* rescue over-proliferative phenotype of *ApoE−/−* neurons

(A) Left: Representative immmunofluorescence images of Day 35 neurons stained with MAP2 and DAPI. The scale bars represent 150 μm. Right: Quantification of MAP2 density, calculated by dividing MAP2-positive area over total numbers of DAPI-stained nuclei. Data presented as mean ± S.D. (2-tailed paired *t*-test).

(B) Relative ROS levels, normalized to protein concentration, in Day 14 and Day 35 neurons. Data presented as mean ± S.D. (n = 3 technical triplicates, ***p < 0.001, 2-tailed *t*-test).

Figure 2. *Continued*

(C) Immunoblot of parental NSC and stable lines infected with either Flag-*ApoE3* or *E4* lentiviral cDNA. Top and bottom arrowhead denote ectopic Flag-ApoE and endogenous ApoE respectively.

(D) Representative immunofluorescence images and (E) quantification of Day 21 neurons subjected to EdU labeling. Neurons were stained with DAPI and MAP2 antibody. Data presented as mean of five microscopy fields ±S.D. (**p = 3e-4; ***p = 3e-5; ##p = 4e-4; #p = 8e-3, 2-tailed *t*-tests). The scale bars represent 150 μm.

(F) Representative immunoblots of lysates from Day 14 and 21 neurons probed with cleaved caspase 3, p21 and actin antibodies.

(G) Left: Representative immmunofluorescence images of Day 35 neurons stained with DAPI, MAP2 and H3phS10 antibodies; the scale bar represents 150 μm. Right: Quantification of H3phS10-stained nuclei per MAP2-positive area. Each circle represents one microscopy field and R is one biological replicate. Data presented as mean ± S.D. (n = 2, 2-tailed *t*-tests).

(H) Left: Representative immunoblots of lysates from Day 35 neurons probed with Parp1, VIM, p21, and pH2Ax antibodies. Right: The level of different markers was normalized to actin and quantified with reference to control neurons. Data presented as mean ± S.E.M (*p < 0.05, **p < 0.005, n = 5. 2-tailed paired *t*-test).

subtypes identified from single-cell sequencing of human ventral midbrain[27] (Figure 1G; Table S2). The top five positively correlated gene sets include the human GABAergic neuron; GABAergic neuroblast, Dopaminergic type 1 (DA1) and 2 (DA2) neurons, and serotonergic neurons.[27] On the other hand, the negatively correlated genes, with lower expression patterns in Day 14 neurons as compared to NSC, were associated with the signatures of highly proliferative undifferentiated cells such as proliferating lung cells,[32] oligodendrocytes precursor cells from the prefrontal cortex[33] and different neuronal progenitors from ventral midbrain.[27] Consistent with the earlier report,[26] the differentiation protocol produced mixed populations of cortical neurons that recapitulate key transcriptomic signatures of *in vivo* neuronal subtypes from the human brain.

ApoE prevents the proliferation of non-neuronal cells in extended culture

To resolve the discrepancy between the level of *MAP2* mRNA and its protein, we performed immunofluorescence staining of neurons at different time-points with MAP2 antibody. The density of MAP2-positive control neurons was modestly higher than *ApoE−/−* neurons at Day 14 (Figure S1E, p = 0.003). This difference became significantly more profound after three weeks of neuronal culture due to the increased numbers of DAPI-labelled *ApoE−/−* cells by Day 35 (Figures 2A and S1E). This suggests that *ApoE−/−* cells continued to proliferate after neuronal differentiation at Day 14. In addition, *ApoE−/−* neuronal cultures exhibited higher ROS levels as compared to control neurons upon MitoSOX staining, which produces red fluorescence when oxidized by mitochondrial superoxide (Figures 2B and S2A).

To investigate the role of ApoE in regulating cell numbers after neuronal differentiation, *ApoE−/−* NSC was first rescued with either *ApoE3* or *ApoE4* by lentiviral infection (Figure 2C). Following the neuronal differentiation of the NSC, the proliferative capacity of different lines was measured by EdU-labelling in Day 21 neurons. Compared to the quiescent control neurons, there were significantly higher numbers of EdU-labelled cells in Day 21 *ApoE−/−* neurons (Figures 2D, 2E, S2B, and S2C). Interestingly, both ApoE3 and ApoE4 reduced the level of EdU-labelling in *ApoE−/−* cells, although ApoE3 appeared to induce higher MAP2 density in Day 21 neurons (Figures 2D, 2E, S2B, and S2C). In aging human mesenchymal progenitor cells, ApoE has been shown to induce senescence by destabilizing heterochromatin.[34] To address any possible contribution of DNA damages, apoptosis, or senescence to the different EdU-labelling index, Day 14 and 21 neurons were probed with γH2Ax, cleaved caspase 3 and p21 antibodies. The levels of γH2Ax, an early cellular response to DNA double-strand breaks,[35] and cellular senescence marker p21,[36] were not significantly different between control and *ApoE−/−* neurons (Figures 2F, S2D, and S2E). Although cleaved caspase 3 was detected in Day 14 neurons and higher in some control biological replicates as compared to *ApoE−/−* (Figure S2E), its level reduced drastically by Day 21 (Figure 2F). These results indicate that the higher level of EdU-labelling observed in *ApoE−/−* neurons at Day 21 was resulted from increased cellular proliferation. Consistent with this notion, staining with the mitotic marker phosphohistone H3 at Ser10 (H3phS10)[37] showed a significant increase in the numbers of H3phS10-positive cells in Day 35 *ApoE−/−* neurons as compared to control (Figure 2G). In addition to over-proliferation, immunoblotting of *ApoE−/−* Day 35 neurons also revealed elevated levels of DNA damage response proteins (Parp1 and γH2Ax),[35] cellular senescence (p21)[36] and epithelial-to-mesenchymal-transition (EMT) marker Vimentin (VIM)[38,39] (Figures 2H and S2F).

The aberrant phenotypes of *ApoE−/−* cells during extended culture of neurons against the backdrop of ApoE expression confined to NSC and NPC suggests that ApoE may act epigenetically during early phases of differentiation to maintain the integrity of mature neurons.

Aberrant gene expression patterns in *ApoE−/−* cells during differentiation

To characterize the underlying transcriptional changes of the observed phenotypes, DESeq2 (adjusted p value <0.05) was used to identify differentially expressed genes between control and *ApoE−/−* cells at the different time-points. Consistent with its reported role as a transcriptional repressor,[20] there were more genes that exhibited higher expression in *ApoE−/−* NSC, Day 14, and Day 35 neurons as compared to control (Figure 3A; Table S3), with a common group of genes associated with extracellular matrix (ECM) organization and angiogenesis (Figure 3B; Tables S3 and S4). Several of these genes, which include Collagen Type XIII α1 chain (*COL13A1*) and Transforming Growth Factor β Induced (*TGFβI*), were validated by qPCR (Figures 3C and S2G). The differentially expressed genes also correlated with the phenotypic differences between control and *ApoE−/−* cells. For instance, silencing of the catalase (*CAT*) gene (Figures 4A and S3A–S3C), which encodes an antioxidant enzyme,[40] might account for the elevated ROS level in *ApoE−/−* cells (Figures 2B and S2A). Similarly, genes highly expressed in *ApoE−/−* neurons were also involved in cell division, positive regulation of fibroblast proliferation and EMT (Figure 3B). Many of these genes, including those associated with cell cycle (*CCNA2*, *MKI67*), cellular senescence (*CCL2*, *BCL2L12*), fibroblasts/EMT (*VIM*, *S100A4*), DNA

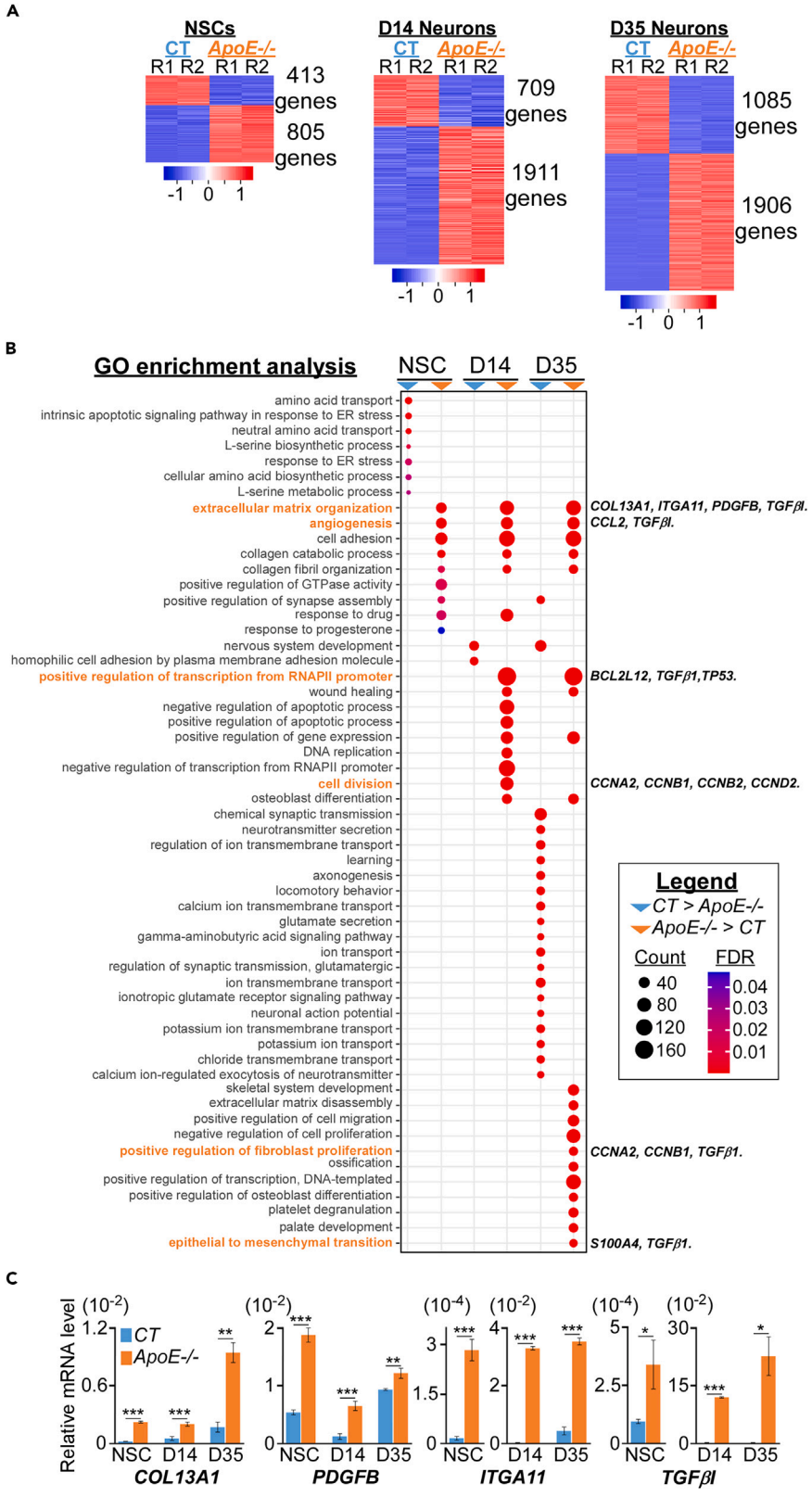
A
NSCs
CT ApoE-/-
R1 R2 R1 R2
413 genes
805 genes
-1 0 1
D14 Neurons
CT ApoE-/-
R1 R2 R1 R2
709 genes
1911 genes
-1 0 1
D35 Neurons
CT ApoE-/-
R1 R2 R1 R2
1085 genes
1906 genes
-1 0 1
B
GO enrichment analysis
NSC D14 D35
amino acid transport
intrinsic apoptotic signaling pathway in response to ER stress
neutral amino acid transport
L-serine biosynthetic process
response to ER stress
cellular amino acid biosynthetic process
L-serine metabolic process
extracellular matrix organization
angiogenesis
cell adhesion
collagen catabolic process
collagen fibril organization
positive regulation of GTPase activity
positive regulation of synapse assembly
response to drug
response to progesterone
nervous system development
homophilic cell adhesion by plasma membrane adhesion molecule
positive regulation of transcription from RNAPII promoter
wound healing
negative regulation of apoptotic process
positive regulation of apoptotic process
positive regulation of gene expression
DNA replication
negative regulation of transcription from RNAPII promoter
cell division
osteoblast differentiation
chemical synaptic transmission
neurotransmitter secretion
regulation of ion transmembrane transport
learning
axonogenesis
locomotory behavior
calcium ion transmembrane transport
glutamate secretion
gamma-aminobutyric acid signaling pathway
ion transport
regulation of synaptic transmission, glutamatergic
ion transmembrane transport
ionotropic glutamate receptor signaling pathway
neuronal action potential
potassium ion transmembrane transport
potassium ion transport
chloride transmembrane transport
calcium ion-regulated exocytosis of neurotransmitter
skeletal system development
extracellular matrix disassembly
positive regulation of cell migration
negative regulation of cell proliferation
positive regulation of fibroblast proliferation
ossification
positive regulation of transcription, DNA-templated
positive regulation of osteoblast differentiation
platelet degranulation
palate development
epithelial to mesenchymal transition
COL13A1, ITGA11, PDGFB, TGFβI.
CCL2, TGFβI.
BCL2L12, TGFβ1,TP53.
CCNA2, CCNB1, CCNB2, CCND2.
CCNA2, CCNB1, TGFβ1.
S100A4, TGFβ1.
Legend
CT > ApoE-/-
ApoE-/- > CT
Count
40
80
120
160
FDR
0.04
0.03
0.02
0.01
C
Relative mRNA level
(10-2)
CT
ApoE-/-
NSC D14 D35
COL13A1
(10-2)
PDGFB
(10-4)
(10-2)
ITGA11
(10-4)
(10-2)
TGFβI

Figure 3. Dysregulated transcriptome in *ApoE*−/− NSC and differentiated neurons

(A) Heatmap of differentially expressed genes between control (CT) and *ApoE*−/− NSC, Day 14 and Day 35 neurons.

(B) Enriched GO terms for differentially expressed genes between control and *ApoE*−/− NSC, Day 14 and Day 35 neurons. Differential expressed genes that contributed to the altered phenotypes of *ApoE*−/− neurons are listed.

(C) qPCR validation of key extracellular matrix (ECM) organization genes elevated across all stages of *ApoE*−/− cells. Data presented as mean ± S.D. (triplicate qPCR reactions, 2-tailed *t*-tests).

damage responses (*H2AX*, *TP53*), and DNA repair pathways (*NHEJ1*, *XRCC6*)[41] were further validated by qPCR (Figures 4A and S3A–S3C, and Table S4). These results indicate that loss of ApoE can lead to the aberrant expression of genes that regulate cell proliferation and EMT during neuronal differentiation. It further raises an intriguing question on how ApoE might facilitate the silencing of non-neuronal genes when its mRNA and protein levels reduced drastically in NPC and became completely undetectable in Day 14 neurons (Figures 1B, 1C, and S1A–S1C).

Reduction of H3K27me3 level in *ApoE*−/− neural progenitor cells and neurons

To gain better insight into its regulatory mechanism, we examined the localization pattern of ApoE and probed for several epigenetic marks between control and *ApoE*−/− cells. Consistent with its reported role as a transcriptional repressor,[20] ApoE was readily detected in the nuclear fraction by western blot (Figure 4B). Similarly, immunofluorescence staining with Lamin B1 and ApoE antibodies showed that ApoE localized mainly to the cytoplasm with traces of nuclear speckles observed in control but not *ApoE*−/− NSC (Figure 4C).

Interestingly, recent studies showed that ApoE may reconfigure the distribution of specific histone marks in different developmental contexts. For instance, ApoE is necessary for H3K27ac deposition at the promoters of immediate-early genes during memory consolidation in mouse neurons[5] while it depletes H3K9me3-marked heterochromatin in aging human mesenchymal progenitor cells.[34] Thus, it is plausible that ApoE may impart the epigenetic silencing of non-neuronal genes via repressive histone marks in the NPC and neurons. Although the H3K9me3 mark was observed to be elevated in *ApoE*−/− Day 35 neurons, its levels fluctuated throughout neuronal differentiation between different biological replicates (Figure S3D). Interestingly, the H3K27me3 level was found to be consistently and significantly higher in the control NPC and differentiated neurons when compared to their *ApoE*−/− counterparts (Figures 4D, S3E, and S3F). To test if this also occurs *in vivo*, hindbrain tissues harvested from male *wildtype* and *ApoE* knockout (KO) mice were probed for H3K27me3 and histone H3. Like the differentiated human neurons, the H3K27me3:H3 ratio in hindbrains from *ApoE* KO mice was significantly lower than its *wildtype* counterparts (Figures 4E and S3G). This suggests that the crosstalk between ApoE and H3K27me3 level within the neuronal population might be evolutionarily conserved.

To further establish the causal link between ApoE expression and H3K27me3 level, we examined the abundance of H3K27me3 by the immunoblot and imaging of *ApoE*−/− NSC and Day 14 neurons that stably expressed ApoE3. In *ApoE*−/− NSC, ectopically expressed ApoE3 was highly enriched in the cytoplasm with punctate nuclear speckles, which colocalized poorly with H3K27me3 staining (Figure 4F). Although the average H3K27me3 level in *ApoE*−/− NSC was shown to be marginally lower as compared to control, the difference was not statistically significant across many biological replicates (Figures 4D and S3E). In accordance, ectopic ApoE3 expression in *ApoE*−/− NSC was unable to increase H3K27me3 level consistently across all biological replicates of NSC (Figures 4F and S3H). On the other hand, when these NSC were differentiated into Day 14 neurons, ectopically expressed ApoE3 was detected in the nucleus and could rescue H3K27me3 level to varying extent in different *ApoE*−/− neurons (Figures 4G and S3I). These results suggest two possibilities. First, it is conceivable that the repressive H3K27me3 mark might be involved in the silencing of non-neuronal genes in the NPC and neurons during which ApoE expression diminished and disappeared. Second, results from *ApoE*−/− cells suggest that ApoE3 expression in NSC is likely needed to impart a high level of H3K27me3 modification at a later stage of differentiation, presumably through intermediary factor(s).

To address the first possibility, we examined if the aberrant expression of the non-neuronal genes, such as those involved in ECM organization and angiogenesis, might be linked to the loss of H3K27me3-mediated repression in *ApoE*−/− NPC. Apart from the *TGFβ1* gene, most of these genes were either repressed or silenced in control as compared to *ApoE*−/− NPC (Figures 5A and S4A). Remarkably, closer examination of genome-wide H3K27me3 ChIP-seq data in control human NSC[42] revealed strong H3K27me3 enrichment either at the promoters or gene bodies of these genes (Figure 5B). To test if differential mRNA expression between control and *ApoE*−/− NPC is correlated to H3K27me3 occupancy, we performed H3K27me3 ChIP-qPCR of these genes. As a negative control, we observed no difference in the level of H3K27me3 occupancy at *TGFβ1* and *NeuroD4*, whose mRNA was expressed similarly between control and *ApoE*−/− NPC. On the other hand, the level of H3K27me3 occupancy was significantly higher at the genes that were repressed or silenced in the control NPC (Figures 5B and S4B). This suggests that H3K27me3-mediated repression might prevent the aberrant expression of these non-neuronal genes in control NPC. Conversely, the reduced H3K27me3 mark likely caused their aberrant expression in *ApoE*−/− cells during differentiation.

We next asked how ApoE may modulate H3K27me3 levels in the NSC/NPC by identifying the possible intermediary factor(s) involved. RNA-sequencing analysis of NSC (Table S3) and qRT-PCR in NPC did not detect any differences in the expression of genes that encode PRC components such as EZH1 (Figure S4C).[43] Unexpectedly, we found that the protein level of EZH1 protein was significantly lower in *ApoE*−/− NPC as compared to control NPC (Figures 5C and S4D). To address if the level of EZH1 protein is directly regulated by *ApoE* expression, we examined its level in *ApoE*−/− NSC rescued with the *Flag-ApoE3* lentiviral construct (Figure 2C). Interestingly, the stable expression of Flag-ApoE3 in *ApoE*−/− NSC increased the level of EZH1 protein (Figure S4E). Although ApoE reverted the patterns of several differentially expressed genes in *ApoE*−/− NSC, it did not affect the *EZH1* mRNA level, suggestive of possible post-transcriptional regulation (Figure S4F). In accordance, stable expression of Flag-ApoE3 also rescued the EZH1 protein level in *ApoE*−/− NPC (Figures 5C and S4G) as well as the density of MAP2-positive neurons at Day 14 (Figures S4H and S4I). Consistent with earlier EdU-labelling result (Figures 2D and S2B),

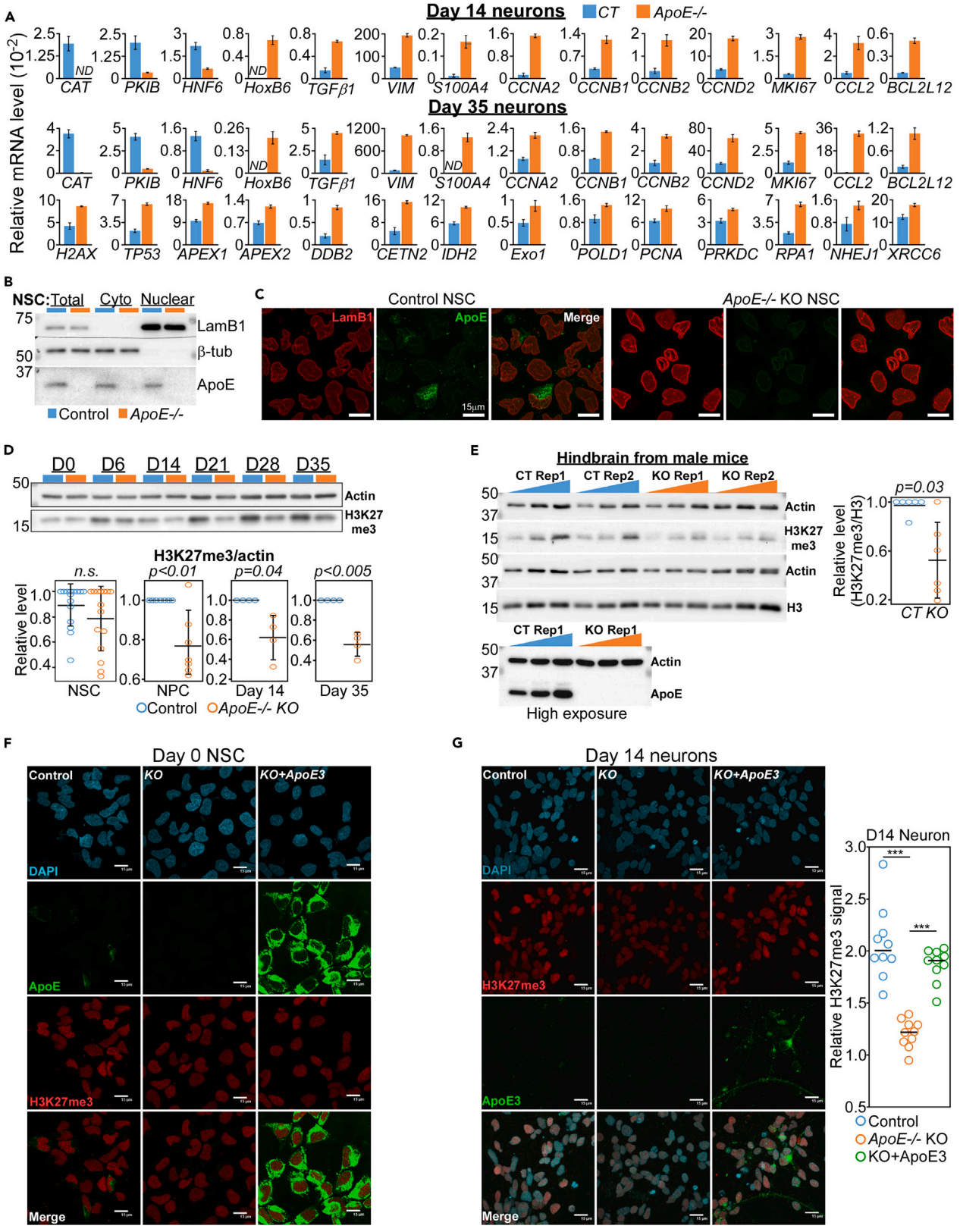
A
Day 14 neurons
CT
ApoE-/-
Relative mRNA level (10-2)
CAT
PKIB
HNF6
HoxB6
TGFβ1
VIM
S100A4
CCNA2
CCNB1
CCNB2
CCND2
MKI67
CCL2
BCL2L12
Day 35 neurons
H2AX
TP53
APEX1
APEX2
DDB2
CETN2
IDH2
Exo1
POLD1
PCNA
PRKDC
RPA1
NHEJ1
XRCC6
ND
B
NSC: Total Cyto Nuclear
LamB1
β-tub
ApoE
Control
ApoE-/-
C
Control NSC
ApoE-/- KO NSC
LamB1
ApoE
Merge
15μm
D
D0 D6 D14 D21 D28 D35
Actin
H3K27 me3
H3K27me3/actin
n.s.
p<0.01
p=0.04
p<0.005
Relative level
NSC
NPC
Day 14
Day 35
Control
ApoE-/- KO
E
Hindbrain from male mice
CT Rep1
CT Rep2
KO Rep1
KO Rep2
Actin
H3K27 me3
H3
ApoE
High exposure
p=0.03
Relative level (H3K27me3/H3)
CT KO
F
Day 0 NSC
Control
KO
KO+ApoE3
DAPI
ApoE
H3K27me3
Merge
G
Day 14 neurons
ApoE3
D14 Neuron
Relative H3K27me3 signal
***
Control
ApoE-/- KO
KO+ApoE3

Figure 4. Dysregulated gene expression with altered H3K27me3 level in *ApoE−/−* human neuronal cells and mouse hindbrain tissues

(A) qPCR validation of differentially expressed genes associated with oxidative stress, cell cycle, celullar senescence, fibroblast proliferation, DNA damage repair in control and *ApoE−/−* neurons. Data presented as mean ± S.D. (triplicate qPCR reactions). All differences are statistically significant ($p < 0.05$, 2-tailed *t*-tests).

(B) Immunoblot of ApoE in the different cellular fractions prepared from control and *ApoE−/−* NSC lysates. β-tubulin and Lamin B1 were used as cytoplasmic (cyto) and nuclear markers respectively.

(C) Representative immunofluorescence images of control and *ApoE−/−* NSC stained for Lamin B1 (red) and ApoE (green). The scale bars represent 15 μm.

(D) Top: Representative immunoblot of control and *ApoE−/−* human neuronal cells harvested on different days "D" with actin and H3K27me3 antibodies. Bottom: H3K27me3 was normalized to actin and quantified with reference to control. Each circle represents one biological replicate. Data presented as mean ± S.D. (2-tailed paired *t*-test).

(E) Immunoblot and quantification of control (CT) and *ApoE* knockout (KO) mouse hindbrains. Tissue lysates were probed with actin, ApoE, H3 and H3K27me3 antibodies. Both H3 and H3K27me3 was normalized to actin and quantified with reference to control. "Rep" stands for one biological replicate. Data presented as mean ± S.D. (2-tailed paired *t*-test).

(F) Representative immunofluorescence images of control, *ApoE−/− KO*, and *ApoE−/− KO* NSC with the stable expression of Flag.ApoE3. Cells were stained with DAPI, ApoE and H3K27me3 antibodies. The scale bar represents 15 μm.

(G) Left: Representative immunofluorescence images of control, *ApoE−/− KO*, and *ApoE−/− KO* with the stable expression of Flag.ApoE3 Day 14 neurons. Cells were stained with H3K27me3 (red) and ApoE (green) antibodies. The scale bar represents 15 μm. Right: Quantification of H3K27me3 fluorescence signal over total H3K27me3-positive area. Each circle represents one microscope field. Data presented as mean ± S.D. (***$p < 8e\text{-}7$, 2-tailed paired *t*-test).

Flag-ApoE3 reduced the percentage of H3phS10-positive cells in Day 14 neurons as compared to *ApoE−/−* culture (Figures S4H and S4J). These results suggest that ApoE3 can upregulate the level of EZH1 protein by post-transcriptional mechanism, which in turn facilitates the H3K27me3-dependent repression of non-neuronal genes in NPC and neurons.

ApoE exerts its epigenetic effect via repressing microRNA levels in neural stem cells and neural progenitor cells

Accumulated data indicate extensive crosstalk between ApoE and miRNAs in different biological contexts. For instance, the expression of many miRNAs was significantly altered in the aortic tissues of *ApoE−/−* mouse, a model for atherosclerosis.[44] Consequentially, the rate of atherosclerosis could be affected by targeting specific miRNAs in these mice.[45–49] ApoE also regulates the transcription of *miR-146a*, which controls the inflammatory response in plasma and the brain.[50] These data suggest that ApoE may regulate EZH1 post-transcriptionally through miRNAs. To test this hypothesis, we performed miRNA sequencing of control and *ApoE−/−* NSC. Annotation with the miRge3.0 pipeline[51] followed by DESeq2 analysis (FDR <0.05) identified 98 differentially expressed miRNAs, of which 55 were elevated in *ApoE−/−* NSC (Figure S5A; Table S5). Using the Encyclopedia of RNA Interactomes (ENCORI) database,[52] we discovered that 15 of the miRNAs significantly upregulated in *ApoE−/−* NSC were computationally predicted to target *EZH1* mRNA (Figures 5D and S5A, and Table S5), including *miR-199a-5p* and *miR-143-3p*. Surprisingly, *miR-199a-5p*, the top hit from our analysis, was previously identified as one of the drivers of melanoma metastasis and angiogenesis through its repression of *ApoE* mRNA.[53] We next validated their expression level in control, *ApoE−/−* and *ApoE−/−* NSC that stably expressed Flag-ApoE3 by qPCR. Compared to control NSC and NPC, the levels of *miR-199a-5p* and *miR143-3p* were significantly elevated in *ApoE−/−* cells but repressed by ectopically expressed Flag-ApoE3 (Figures 5E and S5B).

In melanoma, *miR-199a-5p* represses *ApoE* mRNA by binding to sites B and D on its coding sequences (CDSs) (Figures 5F and S5C).[53] Interestingly, in addition to recognizing its 5′-seed region, multiple sites on *ApoE* CDS were predicted to form energetically stable base-pairing with the 3′-end of *miRNA-199a-5p* (Figures 5F and S5D, and Table S6). As extensive pairing between target mRNA and the 3′-end of miRNA can trigger target-direct miRNA degradation (TDMD),[54–56] we asked if *ApoE* CDS alone is sufficient to repress *miR-199a-5p*. To this end, we deleted the Kozak sequence and start codon from *ApoE* cDNA to make full-length, N-terminal, and C-terminal *ApoExStart* CDS constructs (Figures 5G and S5E). Several independent *ApoE−/−* NSC lines that expressed different versions of *ApoExStart* mRNA were generated by lentiviral infection. Consistent with the removal of the Kozak and start codon, full-length *ApoExStart* constructs expressed a high level of *ApoE* mRNA without being translated into the Flag-ApoE protein (Figures S5F and S5G). Importantly, the expression of either full-length, N-terminal, or C-terminal *ApoExStart* mRNA was sufficient to repress the level of *miR-199a-5p* in *ApoE−/−* NSC (Figures 5H, S5G, and S5H). Taken together, these results indicate that non-translatable *ApoE* mRNA is sufficient to trigger TDMD of *miR-199a-5p*.

To test if *miR-199a-5p* regulates H3K27me3 level through targeting EZH1 in *ApoE−/−* cells (Figure 5I), NC-1 control, *miR-199a-5p* or *miR-143-3p* steric inhibitor were transfected into control and *ApoE−/−* NSC as well as during NPC differentiation. Consistent with earlier data that ectopic ApoE expression has a marginal effect on H3K27me3 level at the NSC stage, administrating *miR-199a-5p* inhibitor led to a statistically significant but only modest increase in the level of H3K27me3 in *ApoE−/−* NSC as compared to NC-1 control (Figure 5J). In line with earlier immunoblot data (Figure 4D), the overall level of H3K27me3 was higher in control as compared to *ApoE−/−* NPC (Figure 5K). Interestingly, inhibitors to both *miR-199a-5p* and *miR-143-3p* led to a more than 1.2-fold increase in the level of H3K27me3 as compared to NC-1 treatment in differentiating *ApoE−/−* NPC (Figure 5K). These results are consistent with the notion that ApoE epigenetically maintains H3K27me3 level by repressing *miR-199a-5p* during neuronal differentiation.

DISCUSSION

Genes highly elevated in cortical neurons after two weeks of *in vitro* differentiation were enriched for GO terms related to neuron development and functions (Figure 1F). Importantly, Day 14 neurons showed remarkable transcriptomic similarity to their *in vivo* counterparts through

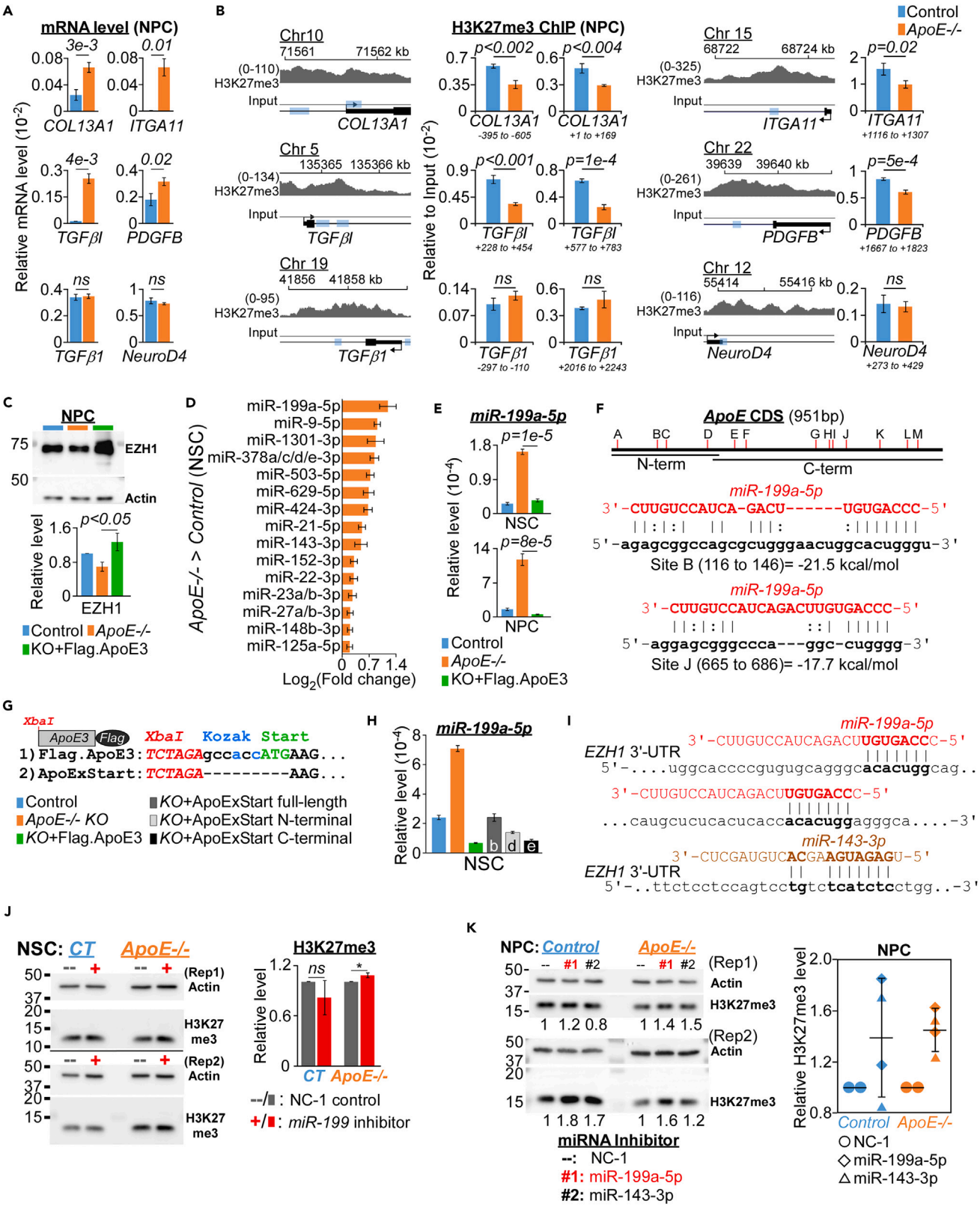
A
mRNA level (NPC)
Relative mRNA level (10-2)
COL13A1
ITGA11
TGFβI
PDGFB
TGFβ1
NeuroD4
B
H3K27me3 ChIP (NPC)
Relative to Input (10-2)
Control
ApoE-/-
Chr10
Chr 5
Chr 19
Chr 15
Chr 22
Chr 12
H3K27me3
Input
C
NPC
EZH1
Actin
Relative level
Control ApoE-/-
KO+Flag.ApoE3
D
ApoE-/- > Control (NSC)
miR-199a-5p
miR-9-5p
miR-1301-3p
miR-378a/c/d/e-3p
miR-503-5p
miR-629-5p
miR-424-3p
miR-21-5p
miR-143-3p
miR-152-3p
miR-22-3p
miR-23a/b-3p
miR-27a/b-3p
miR-148b-3p
miR-125a-5p
Log2(Fold change)
E
miR-199a-5p
Relative level (10-4)
NSC
NPC
F
ApoE CDS (951bp)
N-term
C-term
miR-199a-5p
Site B (116 to 146)= -21.5 kcal/mol
Site J (665 to 686)= -17.7 kcal/mol
G
XbaI
ApoE3 Flag
Kozak Start
1) Flag.ApoE3: TCTAGAgccaccATGAAG...
2) ApoExStart: TCTAGA---------AAG...
Control
ApoE-/- KO
KO+Flag.ApoE3
KO+ApoExStart full-length
KO+ApoExStart N-terminal
KO+ApoExStart C-terminal
H
miR-199a-5p
Relative level (10-4)
NSC
I
miR-199a-5p
EZH1 3'-UTR
miR-143-3p
J
NSC: CT ApoE-/-
(Rep1) Actin
H3K27 me3
(Rep2) Actin
H3K27me3
Relative level
CT ApoE-/-
--/■: NC-1 control
+/■: miR-199 inhibitor
K
NPC: Control ApoE-/-
(Rep1) Actin
H3K27me3
(Rep2) Actin
miRNA Inhibitor
--: NC-1
#1: miR-199a-5p
#2: miR-143-3p
NPC
Relative H3K27me3 level
Control ApoE-/-
NC-1
miR-199a-5p
miR-143-3p

Figure 5. *miR-199a-5p* regulates H3K27me3 occupancy at differentially expressed ECM organization genes in *APOE*−/− NPC

(A) qPCR validation of genes invoved in ECM organization expression in control and *ApoE*−/− NPC. *TGFβ1* and *NeuroD4* were used as negative control. Data presented as mean ± S.D. (triplicate qPCR reactions, 2-tailed *t*-tests). "*ns*" is non-significant.

(B) ChIP-qCR quantification of H3K27me3 occupancy at ECM organization genes. Left: Integrative Genomic Viewers (IGVs) depiction of H3K27me3 distribution across different genes in human NSC as obtained from GSE145964 and GSM4340307. ChIP-qPCR region is highlighted by light blue box. Right: Relative H3K27me3 level is presented as mean ± S.D. (triplicate qPCRs, 2-tailed *t*-test).

(C) Top: Representative immunoblot of control, *ApoE*−/−, and *ApoE*−/− with the stable expression of Flag.ApoE3 NPC for EZH1 and actin. Bottom: EZH1 was normalized to actin and quantified with reference to control NPC. Data presented as mean ± S.E.M. (2-tailed paired *t*-test, n = 3).

(D) List of differentially up-regulated miRNAs in *ApoE*−/− NSC that were predicted to target *EZH1* mRNA. Data presented as Log2(Fold change) ± S.E. (n = 2).

(E) qPCR validation of *miR-199a-5p* expression in control, *ApoE*−/− *KO*, and *ApoE*−/− *KO* with the stable expression of Flag.ApoE3 NSC and NPC. Data presented as mean ± S.D. (triplicate qPCR reactions, 2-tailed *t*-test).

(F) Top: Schematic of the *ApoE* coding sequence (CDS) and the location of predicted *miR-199a-5p* binding sites (denoted as A to M). The N-terminal and C-terminal *ApoE* CDS used for experiment were delineated. Bottom: Predicted base-pairing of either *ApoE* site B or site J with *miR-199a-5p*. Vertical lines indicate Watson-Crick pairing whereas dots indicate G-U wobbles. Predicted free energy was denoted below each RNA duplex.

(G) Schematic of the cloning strategy and color annotated of different *ApoE* CDS used to generate stable NSC lines by lentiviral infection.

(H) Relative level of *miR-199a-5p* in control, *ApoE*−/− and *ApoE*−/− *KO* NSC that stably expressed either Flag.ApoE3 or *ApoE* CDS with deleted Kozak sequence and start codon (*ApoExStart*). "b, d, and e" represent three independent stable lines that expressed full-length, N-terminal and C-terminal non-coding *ApoE* CDS respectively. Data presented as mean ± S.D. (triplicate qPCR reactions; statistically significant difference between *KO* and all *KO* lines that stably expressed different versions of *ApoE* CDS; $p < 2e\text{-}5$, 2-tailed *t*-test).

(I) Schematic of *miR-199a-5p* and *miR-143-3p* binding to the predicted sites on 3′-UTR of *EZH1* mRNA.

(J) Left: Representative immunoblot of control and *ApoE*−/− NSC transfected with either NC-1 or miR-199 inhibitor using actin and H3K27me3 antibodies. "Rep" is biological replicate. Right: Quantification of H3K27me3 level in cells treated with miR-199 inhibitor as compared to NC-1 cells. Data presented as mean ± S.D. (*$p < 0.05$, n = 3, 2-tailed paired *t*-test).

(K) Left: Immunoblot of control and *ApoE*−/− NPC transfected with either NC-1 negative control, inhibitors that target *miR-199a-5p* (diamond) or *miR-143-3p* (triangle) with actin and H3K27me3 antibodies. Numbers indicate the fold change of normalized H3K27me3 level relative to NC-1 transfected NPC. Right: Relative H3K27me3/Actin with reference to NC-1 transfection is indicated for control and *ApoE* −/− NPC. Data presented as mean ± S.D. (statistically significant difference between NC-1 and inhibitors-treated *ApoE*−/− NPC; $p < 0.02$, 2-tailed *t*-test).

GSEA software (Figure 1G). The enrichment of two distinct neurotypes to the *in vitro* differentiated neurons could be explained by the considerable overlap between the transcriptome of dopaminergic and GABAergic neurons.[27]

Both ApoE3 and ApoE4 were sufficient to rescue the over-proliferative phenotype exhibited by *ApoE*−/− Day 21 neurons (Figures 2E and S2C). This is in contrast with the reported allelic effects of *ApoE* where ApoE4 increases the number of mitotic doublecortin-positive cells in the subgranular zone of the Arg-61 mouse model[57] and only ApoE3 can alleviate the inhibitory effect of chemokines on NPC proliferation.[58] Like the *in vitro* differentiation of dentate gyrus granule cell-like hippocampal neurons,[59] the phenotype of differentiated neurons observed in this study was more affected by the absence of *ApoE* rather than different ApoE isoforms.

Indeed, the altered transcriptome and over-proliferation of *ApoE*−/− cells after neuronal differentiation resembled the context of metastasizing melanoma where *miR-199a-5p* represses *ApoE* mRNA.[53] Notably, the metastatic capacity of B16F10 melanoma cells in the mouse model was abrogated by pretreatment with ApoE protein, suggesting that ApoE can impart an anti-angiogenic and metastasis-suppressive memory in these cells.[53] In neuronal context, ApoE expression confined to the NSC and NPC stages (Figures 1A and 1C) appears to elicit H3K27me3-mediated memory during differentiation to repress non-neuronal genes in the mature neurons. Aberrant expression of genes linked to angiogenesis, cell cycle, and DNA damage responses in *ApoE*−/− neuronal culture (Figures 3B, 4A, and S3A–S3C) suggests that ApoE plays crucial roles in regulating cellular proliferation and genome stability across diverse cell types.

Although *miR-199a-5p* was demonstrated to target *ApoE* mRNA,[53] our results support a reciprocal regulatory mechanism. First, the *ApoE* CDS contains multiple binding sites predicted to base-pair with the 3′-end of *miR-199a-5p* outside of its 5′-seed region, which has been demonstrated to be structurally favorable for TDMD (Figures S5C and S5D; Table S6).[54] Second, the ectopic expression of non-translatable full-length, N-terminal, and C-terminal *ApoExStart* mRNAs was sufficient to repress *miR-199a-5p* (Figures 5H, S5G, and S5H). Finally, the role of *ApoE* mRNA in epigenetic regulation is consistent with the relatively low level of nuclear staining of ApoE protein in NSCs (Figures 4C and 4F). Interestingly, *miR-199a-5p* has been shown to function downstream of Methyl-CpG-binding protein 2 (*MeCP2*), whose gene mutations are linked to Rett syndrome (RTT). Mellios and colleagues observed elevated levels of *miR-199a-5p* in MeCP2-deficient neurons that were derived from patients with RTT.[60] Inhibition of *miR-199a-5p* in *MeCP2*-deficient NPC rescued defective neuronal differentiation, while its overexpression in wild-type mouse embryonic brains disrupted early neurogenesis, suggesting that elevated levels of *miR-199a-5p* in RTT can cause aberrant neurodevelopment, much like the phenotypes in *ApoE*−/− neurons. However, *miR-199a-5p* is expressed from two genomic loci, namely *miR-199a-1* and *miR-199a-2*, in mice. It remains unclear why the genetic deletion of *miR-199a-2*, but not *miR-199a-1*, led to some RTT symptoms in mice.[61] Further temporal and spatial analysis of *miR-199a-5p* during brain development will be required to resolve its conflicting roles in driving RTT pathology.

In this study, we showed that ApoE is required to maintain the integrity of differentiated cortical neurons through EZH1-mediated H3K27me3 silencing. Analysis of autopsied healthy and pathological human brains revealed increased the expression of neuronal ApoE in and around ischemic foci, suggesting that ApoE may play protective/regenerative roles in these neurons.[10] Interestingly, pathogenic variants in the *EZH1* gene have been recently identified as the underlying cause of neurodevelopmental disorders in 19 individuals through whole exome sequencing and functional studies.[62] Characterization of different *EZH1* mutations identified in these patients with chick embryo

neural tube and human forebrain organoids showed that EZH1 is both necessary and sufficient for the proper differentiation of NPC into cortical neurons.[62] In addition, translational control of Polycomb component EZH1 by the *ApoE/miR-199a-5p* axis to ensure H3K27me3-mediated repression resembles the role of Fbl, a rRNA methyltransferase, in regulating the temporal progression and differentiation of mouse NSC. Mechanistically, Fbl enhances the translation of Polycomb components EZH2 and Kdm6, which in turn maintain H3K27me3 deposition at many genes required for the proper differentiation of NSCs.[63]

It remains unclear why elevated expression of the EZH1 protein only increased the H3K27me3 level in NPC but not in NSC in our study. It is well-documented that the genomic recruitment and enzymatic activity of the PRC2-EZH1 complex are regulated by several factors, including JARID2, PHF1, MTF2, and AEBP2.[64] Further experiments will be needed to determine if some of these factors are involved in fine-tuning EZH1 activity during different stages of the neuronal differentiation.

Limitations of the study

We demonstrated the importance of ApoE mRNA in maintaining the integrity of mature cortical neurons by TDMD of *miR-199a-5p* through the *in vitro* differentiation of human NSC into neurons. It will be necessary to further validate this mechanism using an *in vivo* mouse model or organoid culture of human NSC. In addition to the ChIP-qPCR of key candidate genes shown in our study, genome-wide profiling of H3K27me3 depositions of control and *ApoE−/−* cells at different stages of the differentiation will provide a clearer picture on how Polycomb-mediated silencing might regulate neuronal programs and maintain the integrity of mature neurons.

STAR★METHODS

Detailed methods are provided in the online version of this paper and include the following:

- KEY RESOURCES TABLE
- RESOURCE AVAILABILITY
  - Lead contact
  - Materials availability
  - Data and code availability
- EXPERIMENTAL MODEL AND STUDY PARTICIPANT DETAILS
  - Animals
  - Cell culture
  - Description of the NSC and day 14 neurons
- METHOD DETAILS
  - Transfection of miRNA inhibitors
  - Western immunoblot analysis
  - Quantification of ROS
  - Nuclear fractionation
  - Mouse brain sample preparation
  - Chromatin immunoprecipitation (ChIP)
  - RNA isolation and RNA-sequencing
  - miRNA detection, differential expression analysis and validation
  - Gene set enrichment analysis (GSEA)
  - Quantitative RT-PCR
  - DNA isolation
  - Molecular cloning
  - Transient transfection and lentiviral transduction
  - Immunofluorescence/EdU measurement of cell proliferation in cell culture
  - Prediction of secondary RNA duplex structure
- QUANTIFICATION AND STATISTICAL ANALYSIS

SUPPLEMENTAL INFORMATION

Supplemental information can be found online at https://doi.org/10.1016/j.isci.2024.109231.

ACKNOWLEDGMENTS

This work has been supported by Temasek Life Sciences Laboratory core funding (3160).

AUTHOR CONTRIBUTIONS

Conceptualization, J.T. and C.T.O.; methodology, J.T. and C.T.O.; formal analysis, J.T., Z.K.N., Y.Y.T., and C.T.O.; investigation, J.T., S.Y.C., V.K.R., and C.T.O.; resources, J.W.W., X.Z., and C.T.O.; data curation, Z.K.N, J.T., and C.T.O.; writing – review and editing, draft: J.T. and C.T.O.; visualization, J.T., Z.K.N., Y.Y.T., and C.T.O.; supervision, J.W.W. and C.T.O.; funding acquisition, C.T.O.

DECLARATION OF INTERESTS

X.Z. serves as the President and CEO at RxCell Inc, US. The rest of the authors declare no competing interests.

Received: May 1, 2023
Revised: December 15, 2023
Accepted: February 9, 2024
Published: February 15, 2024

REFERENCES

1. Chen, Y., Strickland, M.R., Soranno, A., and Holtzman, D.M. (2021). Apolipoprotein E: Structural Insights and Links to Alzheimer Disease Pathogenesis. Neuron *109*, 205–221. https://doi.org/10.1016/j.neuron.2020.10.008.
2. Yamazaki, Y., Zhao, N., Caulfield, T.R., Liu, C.C., and Bu, G. (2019). Apolipoprotein E and Alzheimer disease: pathobiology and targeting strategies. Nat. Rev. Neurol. *15*, 501–518. https://doi.org/10.1038/s41582-019-0228-7.
3. Flowers, S.A., and Rebeck, G.W. (2020). APOE in the normal brain. Neurobiol. Dis. *136*, 104724. https://doi.org/10.1016/j.nbd.2019.104724.
4. Han, S.H., Einstein, G., Weisgraber, K.H., Strittmatter, W.J., Saunders, A.M., Pericak-Vance, M., Roses, A.D., and Schmechel, D.E. (1994). Apolipoprotein E is localized to the cytoplasm of human cortical neurons: a light and electron microscopic study. J. Neuropathol. Exp. Neurol. *53*, 535–544. https://doi.org/10.1097/00005072-199409000-00013.
5. Li, X., Zhang, J., Li, D., He, C., He, K., Xue, T., Wan, L., Zhang, C., and Liu, Q. (2021). Astrocytic ApoE reprograms neuronal cholesterol metabolism and histone-acetylation-mediated memory. Neuron *109*, 957–970.e8. https://doi.org/10.1016/j.neuron.2021.01.005.
6. Yang, C.-P., Gilley, J.A., Zhang, G., and Kernie, S.G. (2011). ApoE is required for maintenance of the dentate gyrus neural progenitor pool. Development *138*, 4351–4362. https://doi.org/10.1242/dev.065540.
7. Li, G., Bien-Ly, N., Andrews-Zwilling, Y., Xu, Q., Bernardo, A., Ring, K., Halabisky, B., Deng, C., Mahley, R.W., and Huang, Y. (2009). GABAergic interneuron dysfunction impairs hippocampal neurogenesis in adult apolipoprotein E4 knockin mice. Cell Stem Cell *5*, 634–645. https://doi.org/10.1016/j.stem.2009.10.015.
8. Tensaouti, Y., Stephanz, E.P., Yu, T.S., and Kernie, S.G. (2018). ApoE Regulates the Development of Adult Newborn Hippocampal Neurons. eNeuro *5*, ENEURO.0155-18.2018. https://doi.org/10.1523/ENEURO.0155-18.2018.
9. Chen, Y., Lomnitski, L., Michaelson, D.M., and Shohami, E. (1997). Motor and cognitive deficits in apolipoprotein E-deficient mice after closed head injury. Neuroscience *80*, 1255–1262. https://doi.org/10.1016/s0306-4522(97)00007-9.
10. Aoki, K., Uchihara, T., Sanjo, N., Nakamura, A., Ikeda, K., Tsuchiya, K., and Wakayama, Y. (2003). Increased expression of neuronal apolipoprotein E in human brain with cerebral infarction. Stroke *34*, 875–880. https://doi.org/10.1161/01.STR.0000064320.73388.C6.
11. Knopman, D.S., Amieva, H., Petersen, R.C., Chételat, G., Holtzman, D.M., Hyman, B.T., Nixon, R.A., and Jones, D.T. (2021). Alzheimer disease. Nat. Rev. Dis. Prim. *7*, 33. https://doi.org/10.1038/s41572-021-00269-y.
12. Brecht, W.J., Harris, F.M., Chang, S., Tesseur, I., Yu, G.Q., Xu, Q., Dee Fish, J., Wyss-Coray, T., Buttini, M., Mucke, L., et al. (2004). Neuron-specific apolipoprotein e4 proteolysis is associated with increased tau phosphorylation in brains of transgenic mice. J. Neurosci. *24*, 2527–2534. https://doi.org/10.1523/JNEUROSCI.4315-03.2004.
13. Shi, Y., Yamada, K., Liddelow, S.A., Smith, S.T., Zhao, L., Luo, W., Tsai, R.M., Spina, S., Grinberg, L.T., Rojas, J.C., et al. (2017). ApoE4 markedly exacerbates tau-mediated neurodegeneration in a mouse model of tauopathy. Nature *549*, 523–527. https://doi.org/10.1038/nature24016.
14. Zhao, N., Liu, C.-C., Van Ingelgom, A.J., Martens, Y.A., Linares, C., Knight, J.A., Painter, M.M., Sullivan, P.M., and Bu, G. (2017). Apolipoprotein E4 Impairs Neuronal Insulin Signaling by Trapping Insulin Receptor in the Endosomes. Neuron *96*, 115–129.e5. https://doi.org/10.1016/j.neuron.2017.09.003.
15. Liu, C.C., Zhao, N., Fu, Y., Wang, N., Linares, C., Tsai, C.W., and Bu, G. (2017). ApoE4 Accelerates Early Seeding of Amyloid Pathology. Neuron *96*, 1024–1032.e3. https://doi.org/10.1016/j.neuron.2017.11.013.
16. Wang, C., Najm, R., Xu, Q., Jeong, D.E., Walker, D., Balestra, M.E., Yoon, S.Y., Yuan, H., Li, G., Miller, Z.A., et al. (2018). Gain of toxic apolipoprotein E4 effects in human iPSC-derived neurons is ameliorated by a small-molecule structure corrector. Nat. Med. *24*, 647–657. https://doi.org/10.1038/s41591-018-0004-z.
17. Zhao, J., Fu, Y., Yamazaki, Y., Ren, Y., Davis, M.D., Liu, C.C., Lu, W., Wang, X., Chen, K., Cherukuri, Y., et al. (2020). APOE4 exacerbates synapse loss and neurodegeneration in Alzheimer's disease patient iPSC-derived cerebral organoids. Nat. Commun. *11*, 5540. https://doi.org/10.1038/s41467-020-19264-0.
18. Lin, Y.-T., Seo, J., Gao, F., Feldman, H.M., Wen, H.-L., Penney, J., Cam, H.P., Gjoneska, E., Raja, W.K., Cheng, J., et al. (2018). APOE4 Causes Widespread Molecular and Cellular Alterations Associated with Alzheimer's Disease Phenotypes in Human iPSC-Derived Brain Cell Types. Neuron *98*, 1141–1154.e7. https://doi.org/10.1016/j.neuron.2018.05.008.
19. Ohkubo, N., Mitsuda, N., Tamatani, M., Yamaguchi, A., Lee, Y.D., Ogihara, T., Vitek, M.P., and Tohyama, M. (2001). Apolipoprotein E4 stimulates cAMP response element-binding protein transcriptional activity through the extracellular signal-regulated kinase pathway. J. Biol. Chem. *276*, 3046–3053. https://doi.org/10.1074/jbc.M005070200.
20. Theendakara, V., Peters-Libeu, C.A., Spilman, P., Poksay, K.S., Bredesen, D.E., and Rao, R.V. (2016). Direct Transcriptional Effects of Apolipoprotein. J. Neurosci. *36*, 685–700. https://doi.org/10.1523/JNEUROSCI.3562-15.2016.
21. Qiu, Z., Hyman, B.T., and Rebeck, G.W. (2004). Apolipoprotein E receptors mediate neurite outgrowth through activation of p44/42 mitogen-activated protein kinase in primary neurons. J. Biol. Chem. *279*, 34948–34956. https://doi.org/10.1074/jbc.M401055200.
22. Gan, H.T., Tham, M., Hariharan, S., Ramasamy, S., Yu, Y.H., and Ahmed, S. (2011). Identification of ApoE as an autocrine/paracrine factor that stimulates neural stem cell survival via MAPK/ERK signaling pathway. J. Neurochem. *117*, 565–578. https://doi.org/10.1111/j.1471-4159.2011.07227.x.
23. Hoe, H.-S., Harris, D.C., and Rebeck, G.W. (2005). Multiple pathways of apolipoprotein E signaling in primary neurons. J. Neurochem. *93*, 145–155. https://doi.org/10.1111/j.1471-4159.2004.03007.x.
24. Zhang, Y., Pak, C., Han, Y., Ahlenius, H., Zhang, Z., Chanda, S., Marro, S., Patzke, C., Acuna, C., Covy, J., et al. (2013). Rapid single-step induction of functional neurons from human pluripotent stem cells. Neuron *78*, 785–798. https://doi.org/10.1016/j.neuron.2013.05.029.
25. Huang, Y.-W.A., Zhou, B., Wernig, M., and Südhof, T.C. (2017). ApoE2, ApoE3, and ApoE4 Differentially Stimulate APP Transcription and Aβ Secretion. Cell *168*, 427–441.e421. https://doi.org/10.1016/j.cell.2016.12.044.

26. Pei, Y., Peng, J., Behl, M., Sipes, N.S., Shockley, K.R., Rao, M.S., Tice, R.R., and Zeng, X. (2016). Comparative neurotoxicity screening in human iPSC-derived neural stem cells, neurons and astrocytes. Brain Res. *1638*, 57–73. https://doi.org/10.1016/j.brainres.2015.07.048.
27. La Manno, G., Gyllborg, D., Codeluppi, S., Nishimura, K., Salto, C., Zeisel, A., Borm, L.E., Stott, S.R.W., Toledo, E.M., Villaescusa, J.C., et al. (2016). Molecular Diversity of Midbrain Development in Mouse, Human, and Stem Cells. Cell *167*, 566–580.e19. https://doi.org/10.1016/j.cell.2016.09.027.
28. Efthymiou, A.G., Steiner, J., Pavan, W.J., Wincovitch, S., Larson, D.M., Porter, F.D., Rao, M.S., and Malik, N. (2015). Rescue of an *in vitro* neuron phenotype identified in Niemann-Pick disease, type C1 induced pluripotent stem cell-derived neurons by modulating the WNT pathway and calcium signaling. Stem Cells Transl. Med. *4*, 230–238. https://doi.org/10.5966/sctm.2014-0127.
29. Sharma, Y., Saha, S., Joseph, A., Krishnan, H., and Raghu, P. (2020). In vitro human stem cell derived cultures to monitor calcium signaling in neuronal development and function. Wellcome Open Res. *5*, 16. https://doi.org/10.12688/wellcomeopenres.15626.1.
30. Liberzon, A., Birger, C., Thorvaldsdóttir, H., Ghandi, M., Mesirov, J.P., and Tamayo, P. (2015). The Molecular Signatures Database (MSigDB) hallmark gene set collection. Cell Syst. *1*, 417–425. https://doi.org/10.1016/j.cels.2015.12.004.
31. Subramanian, A., Tamayo, P., Mootha, V.K., Mukherjee, S., Ebert, B.L., Gillette, M.A., Paulovich, A., Pomeroy, S.L., Golub, T.R., Lander, E.S., and Mesirov, J.P. (2005). Gene set enrichment analysis: a knowledge-based approach for interpreting genome-wide expression profiles. Proc. Natl. Acad. Sci. USA *102*, 15545–15550. https://doi.org/10.1073/pnas.0506580102.
32. Travaglini, K.J., Nabhan, A.N., Penland, L., Sinha, R., Gillich, A., Sit, R.V., Chang, S., Conley, S.D., Mori, Y., Seita, J., et al. (2020). A molecular cell atlas of the human lung from single-cell RNA sequencing. Nature *587*, 619–625. https://doi.org/10.1038/s41586-020-2922-4.
33. Zhong, S., Zhang, S., Fan, X., Wu, Q., Yan, L., Dong, J., Zhang, H., Li, L., Sun, L., Pan, N., et al. (2018). A single-cell RNA-seq survey of the developmental landscape of the human prefrontal cortex. Nature *555*, 524–528. https://doi.org/10.1038/nature25980.
34. Zhao, H., Ji, Q., Wu, Z., Wang, S., Ren, J., Yan, K., Wang, Z., Hu, J., Chu, Q., Hu, H., et al. (2022). Destabilizing heterochromatin by APOE mediates senescence. Nat. Aging *2*, 303–316. https://doi.org/10.1038/s43587-022-00186-z.
35. Mah, L.J., El-Osta, A., and Karagiannis, T.C. (2010). gammaH2AX: a sensitive molecular marker of DNA damage and repair. Leukemia *24*, 679–686. https://doi.org/10.1038/leu.2010.6.
36. Hernandez-Segura, A., Nehme, J., and Demaria, M. (2018). Hallmarks of Cellular Senescence. Trends Cell Biol. *28*, 436–453. https://doi.org/10.1016/j.tcb.2018.02.001.
37. Hendzel, M.J., Wei, Y., Mancini, M.A., Van Hooser, A., Ranalli, T., Brinkley, B.R., Bazett-Jones, D.P., and Allis, C.D. (1997). Mitosis-specific phosphorylation of histone H3 initiates primarily within pericentromeric heterochromatin during G2 and spreads in an ordered fashion coincident with mitotic chromosome condensation. Chromosoma *106*, 348–360. https://doi.org/10.1007/s004120050256.
38. Cheng, F., Shen, Y., Mohanasundaram, P., Lindström, M., Ivaska, J., Ny, T., and Eriksson, J.E. (2016). Vimentin coordinates fibroblast proliferation and keratinocyte differentiation in wound healing via TGF-beta-Slug signaling. Proc. Natl. Acad. Sci. USA *113*, E4320–E4327. https://doi.org/10.1073/pnas.1519197113.
39. Ridge, K.M., Eriksson, J.E., Pekny, M., and Goldman, R.D. (2022). Roles of vimentin in health and disease. Genes Dev. *36*, 391–407. https://doi.org/10.1101/gad.349358.122.
40. Glorieux, C., and Calderon, P.B. (2017). Catalase, a remarkable enzyme: targeting the oldest antioxidant enzyme to find a new cancer treatment approach. Biol. Chem. *398*, 1095–1108. https://doi.org/10.1515/hsz-2017-0131.
41. Jackson, S.P., and Bartek, J. (2009). The DNA-damage response in human biology and disease. Nature *461*, 1071–1078. https://doi.org/10.1038/nature08467.
42. Yan, P., Liu, Z., Song, M., Wu, Z., Xu, W., Li, K., Ji, Q., Wang, S., Liu, X., Yan, K., et al. (2020). Genome-wide R-loop Landscapes during Cell Differentiation and Reprogramming. Cell Rep. *32*, 107870. https://doi.org/10.1016/j.celrep.2020.107870.
43. Piunti, A., and Shilatifard, A. (2021). The roles of Polycomb repressive complexes in mammalian development and cancer. Nat. Rev. Mol. Cell Biol. *22*, 326–345. https://doi.org/10.1038/s41580-021-00341-1.
44. Han, H., Wang, Y.H., Qu, G.J., Sun, T.T., Li, F.Q., Jiang, W., and Luo, S.S. (2013). Differentiated miRNA expression and validation of signaling pathways in apoE gene knockout mice by cross-verification microarray platform. Exp. Mol. Med. *45*, e13. https://doi.org/10.1038/emm.2013.31.
45. Tian, F.J., An, L.N., Wang, G.K., Zhu, J.Q., Li, Q., Zhang, Y.Y., Zeng, A., Zou, J., Zhu, R.F., Han, X.S., et al. (2014). Elevated microRNA-155 promotes foam cell formation by targeting HBP1 in atherogenesis. Cardiovasc. Res. *103*, 100–110. https://doi.org/10.1093/cvr/cvu070.
46. Xu, K., Liu, P., and Zhao, Y. (2017). Upregulation of microRNA-876 Induces Endothelial Cell Apoptosis by Suppressing Bcl-Xl in Development of Atherosclerosis. Cell. Physiol. Biochem. *42*, 1540–1549. https://doi.org/10.1159/000479271.
47. Semo, J., Chernin, G., Jonas, M., Shimoni, S., and George, J. (2019). Deletion of the Mir-106b∼ 25 MicroRNA cluster attenuates atherosclerosis in Apolipoprotein E knockout mice. Lipids Health Dis. *18*, 208. https://doi.org/10.1186/s12944-019-1155-8.
48. Yin, R., Zhu, X., Wang, J., Yang, S., Ma, A., Xiao, Q., Song, J., and Pan, X. (2019). MicroRNA-155 promotes the ox-LDL-induced activation of NLRP3 inflammasomes via the ERK1/2 pathway in THP-1 macrophages and aggravates atherosclerosis in ApoE-/- mice. Ann. Palliat. Med. *8*, 676–689. https://doi.org/10.21037/apm.2019.10.11.
49. Liu, Q.Q., Ren, K., Liu, S.H., Li, W.M., Huang, C.J., and Yang, X.H. (2019). MicroRNA-140-5p aggravates hypertension and oxidative stress of atherosclerosis via targeting Nrf2 and Sirt2. Int. J. Mol. Med. *43*, 839–849. https://doi.org/10.3892/ijmm.2018.3996.
50. Teter, B., LaDu, M.J., Sullivan, P.M., Frautschy, S.A., and Cole, G.M. (2016). Apolipoprotein E isotype-dependent modulation of microRNA-146a in plasma and brain. Neuroreport *27*, 791–795. https://doi.org/10.1097/WNR.0000000000000608.
51. Patil, A.H., and Halushka, M.K. (2021). miRge3.0: a comprehensive microRNA and tRF sequencing analysis pipeline. NAR Genom. Bioinform. *3*, lqab068. https://doi.org/10.1093/nargab/lqab068.
52. Li, J.H., Liu, S., Zhou, H., Qu, L.H., and Yang, J.H. (2014). starBase v2.0: decoding miRNA-ceRNA, miRNA-ncRNA and protein-RNA interaction networks from large-scale CLIP-Seq data. Nucleic Acids Res. *42*, D92–D97. https://doi.org/10.1093/nar/gkt1248.
53. Pencheva, N., Tran, H., Buss, C., Huh, D., Drobnjak, M., Busam, K., and Tavazoie, S.F. (2012). Convergent multi-miRNA targeting of ApoE drives LRP1/LRP8-dependent melanoma metastasis and angiogenesis. Cell *151*, 1068–1082. https://doi.org/10.1016/j.cell.2012.10.028.
54. Sheu-Gruttadauria, J., Pawlica, P., Klum, S.M., Wang, S., Yario, T.A., Schirle Oakdale, N.T., Steitz, J.A., and MacRae, I.J. (2019). Structural Basis for Target-Directed MicroRNA Degradation. Mol. Cell *75*, 1243–1255.e7. https://doi.org/10.1016/j.molcel.2019.06.019.
55. Han, J., LaVigne, C.A., Jones, B.T., Zhang, H., Gillett, F., and Mendell, J.T. (2020). A ubiquitin ligase mediates target-directed microRNA decay independently of tailing and trimming. Science *370*, eabc9546. https://doi.org/10.1126/science.abc9546.
56. Shi, C.Y., Kingston, E.R., Kleaveland, B., Lin, D.H., Stubna, M.W., and Bartel, D.P. (2020). The ZSWIM8 ubiquitin ligase mediates target-directed microRNA degradation. Science *370*, eabc9359. https://doi.org/10.1126/science.abc9359.
57. Adeosun, S.O., Hou, X., Zheng, B., Stockmeier, C., Ou, X., Paul, I., Mosley, T., Weisgraber, K., and Wang, J.M. (2014). Cognitive deficits and disruption of neurogenesis in a mouse model of apolipoprotein E4 domain interaction. J. Biol. Chem. *289*, 2946–2959. https://doi.org/10.1074/jbc.M113.497909.
58. Krathwohl, M.D., and Kaiser, J.L. (2004). Chemokines promote quiescence and survival of human neural progenitor cells. Stem Cell. *22*, 109–118. https://doi.org/10.1634/stemcells.22-1-109.
59. Lee, H., Price, J., Srivastava, D.P., and Thuret, S. (2023). In vitro characterization on the role of APOE polymorphism in human hippocampal neurogenesis. Hippocampus *33*, 322–346. https://doi.org/10.1002/hipo.23502.
60. Mellios, N., Feldman, D.A., Sheridan, S.D., Ip, J.P.K., Kwok, S., Amoah, S.K., Rosen, B., Rodriguez, B.A., Crawford, B., Swaminathan, R., et al. (2018). MeCP2-regulated miRNAs control early human neurogenesis through differential effects on ERK and AKT signaling. Mol. Psychiatr. *23*, 1051–1065. https://doi.org/10.1038/mp.2017.86.
61. Tsujimura, K., Irie, K., Nakashima, H., Egashira, Y., Fukao, Y., Fujiwara, M., Itoh, M., Uesaka, M., Imamura, T., Nakahata, Y., et al. (2015). miR-199a Links MeCP2 with mTOR Signaling and Its Dysregulation Leads to Rett Syndrome Phenotypes. Cell Rep. *12*, 1887–1901. https://doi.org/10.1016/j.celrep.2015.08.028.
62. Gracia-Diaz, C., Zhou, Y., Yang, Q., Maroofian, R., Espana-Bonilla, P., Lee, C.H., Zhang, S., Padilla, N., Fueyo, R., Waxman,

E.A., et al. (2023). Gain and loss of function variants in EZH1 disrupt neurogenesis and cause dominant and recessive neurodevelopmental disorders. Nat. Commun. *14*, 4109. https://doi.org/10.1038/s41467-023-39645-5.

63. Wu, Q., Shichino, Y., Abe, T., Suetsugu, T., Omori, A., Kiyonari, H., Iwasaki, S., and Matsuzaki, F. (2022). Selective translation of epigenetic modifiers affects the temporal pattern and differentiation of neural stem cells. Nat. Commun. *13*, 470. https://doi.org/10.1038/s41467-022-28097-y.
64. Holoch, D., and Margueron, R. (2017). Mechanisms Regulating PRC2 Recruitment and Enzymatic Activity. Trends Biochem. Sci. *42*, 531–542. https://doi.org/10.1016/j.tibs.2017.04.003.
65. Dobin, A., Davis, C.A., Schlesinger, F., Drenkow, J., Zaleski, C., Jha, S., Batut, P., Chaisson, M., and Gingeras, T.R. (2013). STAR: ultrafast universal RNA-seq aligner. Bioinformatics *29*, 15–21. https://doi.org/10.1093/bioinformatics/bts635.
66. Anders, S., Pyl, P.T., and Huber, W. (2015). HTSeq–a Python framework to work with high-throughput sequencing data. Bioinformatics *31*, 166–169. https://doi.org/10.1093/bioinformatics/btu638.
67. Galaxy Community (2022). The Galaxy platform for accessible, reproducible and collaborative biomedical analyses: 2022 update. Nucleic Acids Res. *50*, W345–W351. https://doi.org/10.1093/nar/gkac247.
68. Love, M.I., Huber, W., and Anders, S. (2014). Moderated estimation of fold change and dispersion for RNA-seq data with DESeq2. Genome Biol. *15*, 550. https://doi.org/10.1186/s13059-014-0550-8.
69. Sherman, B.T., Hao, M., Qiu, J., Jiao, X., Baseler, M.W., Lane, H.C., Imamichi, T., and Chang, W. (2022). DAVID: a web server for functional enrichment analysis and functional annotation of gene lists (2021 update). Nucleic Acids Res. *50*, W216–W221. https://doi.org/10.1093/nar/gkac194.
70. Korotkevich, G., Sukhov, V., Budin, N., Shpak, B., Artyomov, M.N., and Sergushichev, A. (2021). Fast gene set enrichment analysis. Preprint at bioRxiv. https://doi.org/10.1101/060012.
71. Stephens, M. (2017). False discovery rates: a new deal. Biostatistics *18*, 275–294. https://doi.org/10.1093/biostatistics/kxw041.
72. Reuter, J.S., and Mathews, D.H. (2010). RNAstructure: software for RNA secondary structure prediction and analysis. BMC Bioinf. *11*, 129. https://doi.org/10.1186/1471-2105-11-129.
73. Zou, J., Sweeney, C.L., Chou, B.K., Choi, U., Pan, J., Wang, H., Dowey, S.N., Cheng, L., and Malech, H.L. (2011). Oxidase-deficient neutrophils from X-linked chronic granulomatous disease iPS cells: functional correction by zinc finger nuclease-mediated safe harbor targeting. Blood *117*, 5561–5572. https://doi.org/10.1182/blood-2010-12-328161.
74. Lie, K.H., Chung, H.C.Y., and Sidhu, K.S. (2012). Derivation, propagation, and characterization of neuroprogenitors from pluripotent stem cells (hESCs and hiPSCs). Methods Mol. Biol. *873*, 237–246. https://doi.org/10.1007/978-1-61779-794-1_15.
75. Swistowski, A., Peng, J., Han, Y., Swistowska, A.M., Rao, M.S., and Zeng, X. (2009). Xeno-free defined conditions for culture of human embryonic stem cells, neural stem cells and dopaminergic neurons derived from them. PLoS One *4*, e6233. https://doi.org/10.1371/journal.pone.0006233.
76. Swistowski, A., Peng, J., Liu, Q., Mali, P., Rao, M.S., Cheng, L., and Zeng, X. (2010). Efficient generation of functional dopaminergic neurons from human induced pluripotent stem cells under defined conditions. Stem Cell. *28*, 1893–1904. https://doi.org/10.1002/stem.499.
77. Shaltouki, A., Peng, J., Liu, Q., Rao, M.S., and Zeng, X. (2013). Efficient generation of astrocytes from human pluripotent stem cells in defined conditions. Stem Cell. *31*, 941–952. https://doi.org/10.1002/stem.1334.
78. Efthymiou, A., Shaltouki, A., Steiner, J.P., Jha, B., Heman-Ackah, S.M., Swistowski, A., Zeng, X., Rao, M.S., and Malik, N. (2014). Functional screening assays with neurons generated from pluripotent stem cell-derived neural stem cells. J. Biomol. Screen *19*, 32–43. https://doi.org/10.1177/1087057113501869.
79. Schmidt, S.I., Bogetofte, H., Ritter, L., Agergaard, J.B., Hammerich, D., Kabiljagic, A.A., Wlodarczyk, A., Lopez, S.G., Sørensen, M.D., Jørgensen, M.L., et al. (2021). Microglia-Secreted Factors Enhance Dopaminergic Differentiation of Tissue- and iPSC-Derived Human Neural Stem Cells. Stem Cell Rep. *16*, 281–294. https://doi.org/10.1016/j.stemcr.2020.12.011.
80. Okarmus, J., Bogetofte, H., Schmidt, S.I., Ryding, M., García-López, S., Ryan, B.J., Martínez-Serrano, A., Hyttel, P., and Meyer, M. (2020). Lysosomal perturbations in human dopaminergic neurons derived from induced pluripotent stem cells with PARK2 mutation. Sci. Rep. *10*, 10278. https://doi.org/10.1038/s41598-020-67091-6.
81. Bogetofte, H., Jensen, P., Okarmus, J., Schmidt, S.I., Agger, M., Ryding, M., Nørregaard, P., Fenger, C., Zeng, X., Graakjær, J., et al. (2019). Perturbations in RhoA signalling cause altered migration and impaired neuritogenesis in human iPSC-derived neural cells with PARK2 mutation. Neurobiol. Dis. *132*, 104581. https://doi.org/10.1016/j.nbd.2019.104581.
82. Bogetofte, H., Jensen, P., Ryding, M., Schmidt, S.I., Okarmus, J., Ritter, L., Worm, C.S., Hohnholt, M.C., Azevedo, C., Roybon, L., et al. (2019). PARK2 Mutation Causes Metabolic Disturbances and Impaired Survival of Human iPSC-Derived Neurons. Front. Cell. Neurosci. *13*, 297. https://doi.org/10.3389/fncel.2019.00297.
83. Kayama, T., Suzuki, I., Odawara, A., Sasaki, T., and Ikegaya, Y. (2018). Temporally coordinated spiking activity of human induced pluripotent stem cell-derived neurons co-cultured with astrocytes. Biochem. Biophys. Res. Commun. *495*, 1028–1033. https://doi.org/10.1016/j.bbrc.2017.11.115.
84. Ngian, Z.K., Tan, Y.Y., Choo, C.T., Lin, W.Q., Leow, C.Y., Mah, S.J., Lai, M.K.P., Chen, C.L.H., and Ong, C.T. (2022). Truncated Tau caused by intron retention is enriched in Alzheimer's disease cortex and exhibits altered biochemical properties. Proc. Natl. Acad. Sci. USA *119*, e2204179119. https://doi.org/10.1073/pnas.2204179119.
85. Shaltouki, A., Sivapatham, R., Pei, Y., Gerencser, A.A., Momčilović, O., Rao, M.S., and Zeng, X. (2015). Mitochondrial alterations by PARKIN in dopaminergic neurons using PARK2 patient-specific and PARK2 knockout isogenic iPSC lines. Stem Cell Rep. *4*, 847–859. https://doi.org/10.1016/j.stemcr.2015.02.019.
86. Rao, V.K., Swarnaseetha, A., Tham, G.H., Lin, W.Q., Han, B.B., Benoukraf, T., Xu, G.L., and Ong, C.T. (2020). Phosphorylation of Tet3 by cdk5 is critical for robust activation of BRN2 during neuronal differentiation. Nucleic Acids Res. *48*, 1225–1238. https://doi.org/10.1093/nar/gkz1144.

STAR★METHODS

KEY RESOURCES TABLE

REAGENT or RESOURCE	SOURCE	IDENTIFIER
Antibodies		
Anti-B-actin	Sigma	Cat#A2228; RRID:AB_476697
Anti-MAP2	Santa Cruz	Cat#sc74421; RRID:AB_1126215
Anti-MAP2	Merck	Cat#MAB3418; RRID:AB_94856
Anti-ApoE	Santa Cruz	Cat#sc13521; RRID:AB_626691
Anti-ApoE	Abcam	Cat#ab1906; RRID:AB_302668
Anti-ApoE	Cell Signalling Technology	Cat#68587; RRID: AB_3094528
Anti-ApoE	Cell Signalling Technology	Cat#74417; RRID: AB_3094529
Anti-H3ser10ph	Merck	Cat#06-570; RRID:AB_310177
Anti-PARP1 C-term	Active Motif	Cat#39561; RRID:AB_2793258
Anti-Vimentin	Santa Cruz	Cat#sc6260; RRID:AB_628437
Anti-p21 (Waf/Cip1)	Cell Signalling Technology	Cat#2947S; RRID: AB_823586
Anti-pH2AX	Santa Cruz	Cat#sc517348; RRID:AB_2783871
Anti-Cleaved caspase 3	Cell Signalling Technology	Cat#9661; RRID:AB_2341188
Anti-Histone H3	Abcam	Cat#ab1791; RRID:AB_302613
Anti-Lamin B1	Abcam	Cat#ab16048; RRID:AB_443298
Anti-Lamin B1	Proteintech	Cat#12987-1-AP; RRID:AB_2136290
Anti-Beta-tubulin	Sigma	Cat#T8328; RRID:AB_1844090
Anti-H3K9me3	Abcam	Cat#ab8898; RRID:AB_306848
Anti-H3K27me3	Active Motif	Cat#39155; RRID:AB_2561020
Anti-EZH1	Santa Cruz	Cat#sc515817; RRID: AB_3094531
Anti-FLAG M2	Sigma	Cat#F1804; RRID:AB_262044
Alexa Fluor® 488 AffiniPure Goat Anti-Mouse IgG (H+L)	Jackson Immunoresearch	Cat#115-585-003; RRID:AB_2338871
Cy™3 AffiniPure Goat Anti-Rabbit IgG (H+L)	Jackson Immunoresearch	Cat#111-165-003; RRID:AB_2338000
Goat anti-Mouse IgG (H+L) Secondary Antibody, HRP	Invitrogen	Cat#A16066; RRID:AB_2534739
Goat anti-Rabbit IgG (H+L) Secondary Antibody, HRP	Invitrogen	Cat#A16096; RRID:AB_2534770
Chemicals, peptides, and recombinant proteins		
poly-L-ornithine hydrobromide	Sigma	Cat#P3655
Laminin	Life Technologies	Cat#23017-015
Critical commercial assays		
Neural stem cell maintenance medium	XCell Science Inc.	Cat#SM-001-BM100
Neural stem cell maintenance supplement A	XCell Science Inc.	Cat#SM-001-SA100
Neural stem cell maintenance supplement B	XCell Science Inc.	Cat#SM-001-SB100
Neuron induction medium	XCell Science Inc.	Cat#NI-001-BM100
Neuron induction supplement A	XCell Science Inc.	Cat#NI-001-SA100
Neuron induction supplement B	XCell Science Inc.	Cat#NI-001-SB100
Neuron induction supplement C	XCell Science Inc.	Cat#NI-001-SC100
Neuronal maturation medium	XCell Science Inc.	Cat#NM-001-BM
Neuronal maturation supplement A	XCell Science Inc.	Cat#NM-001-SA100
Lipofectamine™ RNAiMAX Transfection Reagent	Thermofisher Scientific	Cat#13778150
MitoSOX™ Red Mitochondrial Superoxide Indicator	Invitrogen	Cat#M36008

(*Continued on next page*)

Continued

REAGENT or RESOURCE	SOURCE	IDENTIFIER
High-Capacity cDNA Reverse Transcription Kit	Applied Biosystems	Cat#4368814
Click-iT™ Plus EdU Cell Proliferation Kit for Imaging, Alexa Fluor™ 594 dye	Thermo Scientific	Cat#C10639
Lenti-X™ Bicistronic Expression System (Puro)	Clontech	Cat#632183
Deposited data		
Raw and analyzed RNA-seq and miRNA-seq data	This paper	GEO: GSE198245
NSC H3K27me3 ChIP data	Yan et al.[42]	GEO: GSE145964
Experimental models: Cell lines		
Control neural stem cell line XCL-1	XCell Science Inc.	Cat#SC-001-1V
ApoE-/- neural stem cell line	XCell Science Inc.	Cat#SC-001-ZOG-B-1V
Experimental models: Organisms/strains		
C57BL/6J mice	Jackson Laboratory (Maine, USA)	Strain #:000664 RRID: IMSR_JAX:000664
ApoE knockout (ApoE-/-) mice (B6.129P2-Apoetm1Unc/J)	Jackson Laboratory (Maine, USA)	Strain #:002052, RRID: IMSR_JAX:002052
Oligonucleotides		
Full list of primers in Table S7	This paper	N/A
Anti hsa-miR-199a-5p miRNA inhibitor	IDT	Sequence: mG/ZEN/mAmAmCm AmGmGmUmAmGmUmCmUm GmAmAmCmAmCmU mGmG/3ZEN/
Anti hsa-miR-143-3p miRNA inhibitor	IDT	Sequence: mG/ZEN/mAmGmCm UmAmCmAmGmUmGmCmUmUm CmAmUmCmUmC/3ZEN/
NC1 negative control miRNA inhibitor	IDT	Sequence: mG/ZEN/mCmGmUmAm UmUmAmUmAmGmCmCmGmAm UmUmAmAmCmG/3ZEN/
Recombinant DNA		
APOE cDNA ORF clone, Homo sapiens(human)	Genscript	Cat#OHu27296
pLVX-C-term-Flag-IRES-puro lentiviral vector	This paper	Available upon request
pLVX-ApoE3-C-term-Flag-IRES-puro	This paper	Available upon request
pLVX-ApoE4-C-term-Flag-IRES-puro	This paper	Available upon request
pLVX-ApoE3xStart-C-term-Flag-IRES-puro	This paper	Available upon request
pLVX-ApoE3xStart_N-C-term-Flag-IRES-puro	This paper	Available upon request
pLVX-ApoE3xStart_C-C-term-Flag-IRES-puro	This paper	Available upon request
Software and algorithms		
STAR (v2.5)	Dobin et al.[65]	http://code.google.com/p/rna-star/
HTSeq-count	Anders et al.[66]	https://htseq.readthedocs.io/en/release_0.11.1/count.html
Galaxy platform, DESeq2 (v1.22.1) and Heatmap2 (v3.0.1)	The Galaxy Community.[67] Love et al.[68]	https://usegalaxy.org/
DAVID Functional Annotation Bioinformatics (v6.8)	Sherman et al.[69]	https://david.ncifcrf.gov/
miRge3.0	Patil & Halushka[51]	https://github.com/mhalushka/miRge3.0
MSigDB	Liberzon et al.[30] Subramanian et al.[31]	https://www.gsea-msigdb.org/gsea/msigdb/
fgsea R package	Korotkevich et al.[70]	https://bioconductor.org/packages/release/bioc/html/fgsea.html
Shrinkage estimator *ashr*	Stephens[71]	https://github.com/stephens999/ashr
RNAstructure	Reuter & Mathews[72]	https://rna.urmc.rochester.edu/RNAstructure.html

RESOURCE AVAILABILITY

Lead contact

Further information and request for resources and reagents should be directed to and will be fulfilled by the lead contact, Chin-Tong Ong (chintong@tll.org.sg).

Materials availability

Recombinant plasmids generated in this study will be made available from the lead contact upon request.

Data and code availability

- RNA-seq data have been deposited at GEO and are publicly available as of the date of publication. Accession number is listed in the key resources table.
- This paper does not report original code.
- Any additional information required to reanalyse the data reported in this study is available from the lead contact upon request.

EXPERIMENTAL MODEL AND STUDY PARTICIPANT DETAILS

Animals

C57BL/6J and *ApoE* knockout (*ApoE-/-*) mice were purchased from InVivos (Singapore) and Jackson Laboratory (Maine, USA) respectively. Mice were housed under specific pathogen-free conditions with a 12/12-hour light-dark cycle at the Comparative Medicine Animal Vivarium at the National University of Singapore. Mice were given *ad libitum* access to standard chow diet and water. All studies were approved by the National University of Singapore Institutional Animal Care and Use Committee and conformed to the guidelines on the care and use of animals for scientific purposes (NACLAR, Singapore, 2004) and the Guide for the Care and Use of Laboratory Animals published by the US National Institutes of Health (NIIH Publication, 8th Edition, 2011). Brains were harvested from four weeks old adult male mice for western blot analysis.

Cell culture

Isogenic control (XCL-1, SC-001-1V) and *ApoE-/-* NSC (SC-001-ZOG-B-1V) lines were purchased from XCell Science Inc. and described in the next section.

NSC was passaged on Matrigel (Corning #354277) coated plate in NSC maintenance medium (SM-001-BM100) containing maintenance supplement A and B (SM-001-SA100/SB100). Neuronal differentiation was performed according to manufacturer's protocol (XCell Science Inc.).[26] Briefly, NSC were seeded on Day 0 (D0) at a density of 0.04×10^6 cells/cm^2 on plate pre-coated with poly-L-ornithine hydrobromide (20 μg/mL; Sigma P3655) & laminin (10 μg/mL; Life Technologies 23017-015) in NSC maintenance media. Cells were replenished with fresh neuronal induction media containing induction supplement A, B and C (NI-001-BM/SA/SB/SC100) on the next day (Day 1), followed by Day 3 and Day 5. On Day 6 (D6), the induced NPC were detached using accutase (Gibco A1110501), counted, and replated on poly-L-ornithine hydrobromide/laminin-coated 12-well plates at $0.04x10^6$ cells/cm^2 in neuronal maturation medium containing maturation supplement A (NM-001-BM/SA100). Cells were replenished with neuronal maturation media every alternate day until the differentiated neurons were harvested or imaged on Day 14, 21, 28 or 35.

Description of the NSC and day 14 neurons

XCL (XCell Science Inc.) is a subclone of the NCRM1 integration-free male control human induced pluripotent stem cell (iPSC) line (NIH Centre for Regenerative Medicine) described in previous studies.[73,74] (https://www.xcellscience.com/products/nsc).

Isogenic control XCL-1 NSC (XCell Science Inc., SC-001-1V) was developed from XCL iPSC using rosette methodology with StemPro defined media (minus FGF2) and other chemicals as described previously.[75,76] The purity and differentiation efficiency of the NSC were demonstrated subsequently in several studies.[29,77–82]

Neuronal differentiation of NSC using XCell Scince Inc. protocol and detailed characterization of the cortical neurons were previously described.[26] The differentiation protocol has also been used in other studies.[83,84] Gene expression profiles of Day 14 cortical neurons showed high degree of similarity with Ngn-2 induced excitatory cortical neurons,[24] which have been used to study the functional differences between ApoE3 and ApoE4.[18,25] First, 12 out of 13 neuronal markers tested by immunoblot in excitatory cortical neurons (in Figure 2C from Zhang et al., 2013) were differentially expressed in the XCell Day 14 neurons as compared to XCell Day 0 NSC (Table S1, sheet 1). Second, 62 out of 69 neuronal mRNAs tested by single-cell quantitative RT-PCR (in Figure 3A; Table S1 from Zhang et al., 2013) were detected in our NSC and D14 neurons, with majority of them as differentially expressed genes. For instance, NPC markers (NES, Pax6, Sox2) were highly expressed in NSC whereas pan-neuronal markers were mostly elevated in Day 14 neurons (Table S1, sheet 1).

ApoE-/- NSC (SC-001-ZOG-B-1V) line was generated with Zinc Finger Nuclease (ZFN) technology that was previously used to mutate *PARK2* gene.[85] Frame-shift mutations were introduced into the two alleles of *ApoE* gene in isogenic control NSC line. Mutation in allele 1 was achieved by insertion of GAGC immediately after C nucleotide at position 44908639. Mutation in allele 2 involved similar GAGC insertion

together with the deletion of AGC from position 44908637 to 44908639. In this study, RNA-seq, qPCR, western blot and immunohistochemistry did not detect *ApoE* RNA or its protein in *ApoE-/-* cells.

METHOD DETAILS

Transfection of miRNA inhibitors

NSC seeded at a density of 0.1×10^6 cells/well in 24-well Matrigel-coated plates were transfected 24 hours later with 2.5 pmol/well (25 nM final concentration) of miRNA inhibitors against either miR-199a-5p or miR-143-3p using Lipofectamine™ RNAiMAX Transfection Reagent as per the manufacturer's instructions (Thermofisher Scientific). The NSC maintenance medium was replaced 8 hours after transfection. The NSC were harvested 48 hours after transfection. For NPC experiment, NSC were seeded (Day 0) at a density of 0.1×10^6 cells/well in 24-well poly-ornithine & laminin-coated plates. The cells were transfected 24 hours later (on Day 1) and replenished with fresh neuronal induction media 8 hours post-transfection. A second transfection and subsequent media change was performed on Day 3. Following media change on Day 5, NPC were harvested on Day 6 for analysis.

Western immunoblot analysis

Lysates boiled in Laemmli buffer were resolved by SDS-PAGE and transferred to PVDF membranes (Millipore) in Tris-glycine transfer buffer and 20% methanol for 2 hr at 100 V. After blocking with 5 % skim milk or BSA in 1× TBST buffer (20mM Tris, pH7.4, 150 mM NaCl, 0.05% Tween 20), membranes were incubated overnight with primary antibody (detailed in key resources table). Membranes were washed thrice with TBST and incubated with secondary antibody conjugated to HRP (1:3000, Novex, Invitrogen) in blocking buffer for 1 hr. Following three rounds of TBST washes, proteins were assayed using SuperSignal West Pico/Dura Chemiluminescent substrate (Thermofisher Scientific). Quantification was performed with "record measurements" in Adobe Photoshop.

Quantification of ROS

Cell pellets were resuspended in 200 µl of ice-cold PBS containing protease inhibitor cocktail (Roche) and sonicated for 6 cycles (15 s ON/OFF, high power settings) using Bioruptor (UCD-200TO). After sonication, 20 µl of cellular lysate was mixed with 300 µl of 5 µM MitoSOX™ (Invitrogen) and incubated for 10 min at room temperature. For each sample, triplicates of 100 µl of the mixture were measured using a Tecan Spark Multimode Reader at 510 nm excitation and 580 nm emission. The average fluorescence readings were normalized to the total protein concentration of the lysate which was determined by Bicinchoninic acid assay (Bio-Rad).

Nuclear fractionation

Nuclear fractionation was performed as per previous protocol.[86] One million NSC were first resuspended in 400 µL of cold NBA buffer (85 mM NaCl, 5.5% sucrose,10 mM Tris pH 7.5, 0.2 mM EDTA, 1 mM DTT, 1× Roche cOmplete™ Protease Inhibitor Cocktail), followed by the addition of 400 µL of cold NBA + 0.2% of NP-40 buffer. After rocking on ice for 10 min, 80 µL of the mixture was harvested as the "Total" fraction. The remainder was centrifuged at 2000 g for 3 min at 4°C to obtain the "Cytoplasmic" supernatant and "Nuclei" pellet. The pellet was washed twice in NBR buffer (85 mM NaCl, 5.5% sucrose,10 mM Tris pH 7.5, 3 mM $MgCl_2$, 1.5 mM $CaCl_2$, 1 mM DTT, 1× Roche cOmplete™ Protease Inhibitor Cocktail) by centrifugation at 2000 g for 3 min at 4°C. The different fractions were boiled in Laemmli buffer for Western blotting.

Mouse brain sample preparation

Four weeks old male mice euthanized with an overdose of isoflurane (5%) were perfused using 10 mL of ice-cold phosphate buffer saline. The brains were excavated from the skull and then snap-frozen in liquid nitrogen and kept at -80°C. Frozen brain tissues were homogenised in RIPA buffer supplemented with protease inhibitors cocktail (Roche). The lysates were boiled with 6× Laemmli buffer and subjected to immunoblotting.

Chromatin immunoprecipitation (ChIP)

20e6 cells per sample were fixed in 10 mL of Advanced DMEM containing 1% formaldehyde for 10 min with nutation at room temperature. The sample was then quenched by the addition of glycine to a final concentration of 0.125 M and further nutation at room temperature for 5 min. The sample was then centrifuged at 1350xg, 4°C for 5 min. After discarding the supernatant, the pellet washed with 1x PBS. Following another round of centrifugation, the pellet was stored at -80°C prior to use. Each sample pellet was thawed and resuspended in 5 mL of cell lysis buffer (10 mM Tris pH 8.0, 0.25% Triton-X, 10 mM EDTA, 0.1 M NaCl), then Dounce homogenized 10 x using pestle A. After that, the sample was nutated on ice for 10 min before being spun down at 1350xg, 4°C for 5 min. The supernatant was aspirated, and the pellet resuspended in 0.6 mL nuclear lysis buffer (50 mM Tris pH 8.0, 150 mM NaCl, 10 mM EDTA, 1% SDS, 0.1% sodium deoxycholate). The sample was then Dounce homogenized 10x using pestle B, and nutated on ice for 10 min. Next, the sample was sonicated in a Diagenode Bioruptor using the following settings: High power, ON for 0.5 min, OFF for 1 min, for 15 min per cycle, for 7 cycles. The sample was then spun down at 16,000xg, 4°C for 10 min and the supernatant was transferred into a new 15 mL tube. This supernatant was then diluted with the addition of 4.5 mL of ChIP dilution buffer (16.7 mM Tris pH 8.0, 1.2 mM EDTA, 1.1% Triton-X, 0.01% SDS, 167 mM NaCl). 500 µL of this mixture was aliquoted and stored at 4°C as input. 5 µL of Anti-H3K27me3 antibody (Active Motif) was added to the rest of the mixture, which was then incubated with nutation at 4°C overnight. On the same day, 50 µL of Dynabeads™ Protein G were washed in 1mL of blocking buffer

(0.5% w/v BSA, 1x PBS) thrice and stored in an additional 1 mL of blocking buffer at 4°C. The next day, the Dynabeads were captured on a magnetic stand, the blocking buffer discarded, and the beads transferred into the sample mixture, which was then incubated with nutation at 4°C for 6 hours. Following this, the beads were captured, and the supernatant discarded. The beads were then washed by resuspending them in 1 mL RIPA wash buffer (50 mM HEPES, 500 mM LiCl, 1 mM EDTA, 1% NP-40, 0.7% sodium deoxycholate), nutating on ice for 5 min, recapturing the beads and changing the wash buffer. After 5 washes with RIPA wash buffer, the beads were resuspended in 1 mL of TE + NaCL buffer (10 mM Tris pH 8.0, 1mM EDTA, 50mM NaCl) and washed once. The washed beads were then resuspended in 260 μL of elution buffer (50 mM Tris pH 8.0, 10 mM EDTA, 1% SDS) and incubated in a 65°C water bath for 30 min with periodic mixing every 5 minutes. The beads were captured, and the resultant eluate taken for later steps. 10 μL of 5M NaCl and 2.5 μL proteinase K (0.2 mg/mL final concentration) were each added to 250 uL of the input as well as the eluate, and these were then incubated at 65°C overnight. Both samples were then treated with 1.25 μL RNAse A (0.2 μg/mL final concentration) and incubated at 37°C for an hour. The samples were then phenol-chloroform/chloroform-extracted and the DNA ethanol-precipitated. In short, an equal volume of 25:24:1 phenol-chloroform-isoamyl alcohol (250 μL) was added to each sample, vortexed strongly to mix, then spun down at max speed at room temperature, and the upper aqueous layer was transferred into a new tube. This entire process was repeated once but with chloroform instead of phenol-chloroform. After that, 2 volumes of 100% ethanol and 1 μL of 20 mg/mL glycogen was added to the isolated aqueous phase, mixed thoroughly by inverting, and incubated at -20°C for an hour. The precipitated DNA was spun down at max speed, room temperature for 10 min to pellet the DNA, the supernatant discarded, and the pellet washed with 70% ethanol. After another spin at max speed, room temperature for 3 min, the ethanol was carefully and completely removed. The DNA pellets were air-dried briefly before being dissolved in sterile DNAse-free water and stored at -20°C.

RNA isolation and RNA-sequencing

Total RNA from different biological replicates were isolated using RNAzol®RT (Sigma-Aldrich) and RNA-sequencing were carried out by NovogeneAIT (Singapore) according to company protocols.

To determine expression of protein-coding genes, poly-A capture mRNAs were used for library preparation and subjected 150 bp paired-end sequencing. Sequenced reads were aligned to human reference genome (GRCh38.p13) using STAR (v2.5).[65] HTSeq-count was used to identify read counts per gene.[66] Differentially expressed genes were determined using DESeq2 (v1.22.1) on Galaxy platform and visualised by Heatmap2 (v3.0.1).[67,68] Gene Ontology analysis was performed using DAVID Functional Annotation Bioinformatics (v6.8).[69]

Small RNA sequencing was employed to determine expression of miRNAs. Briefly, small RNA library was constructed and subjected to 50 bp single-end sequencing. Annotation of miRNAs are described below.

miRNA detection, differential expression analysis and validation

miRNAs were annotated using miRge3.0 pipeline.[51] It aligned the raw Fastq reads against specific human small-RNA annotation libraries with the following command: miRge3.0 -s -lib miRge3_Lib -on human -db miRBase -o output_dir -gff -trf -ai -cpu 12 -a AGATCGGAAGAGCAC ACGTCTGAACTCC. Differential expression analysis was then performed using DESeq2 on the raw miRNA read counts extracted from miR. Counts_Raw.csv files. miRNA levels were validated using an adapted protocol.[5] Briefly, DNaseI-treated total RNA was precipitated with isopropanol in the presence of 3M NaOAc and linear acrylamide. Poly-A tailing was carried out with *E. coli* Poly(A) Polymerase (NEB) on 2 μg of RNA. Following heat inactivation at 65°C, the miRNA cDNA library was generated using High-Capacity cDNA Reverse Transcription Kit (Applied Biosystems) in the presence of the miRNA anchor primer 5'- CGACTCGATCCAGTCTCAGGGTCCGAGGTATTCGATCGAGTCGC ACTTTTTTTTTTTTV-3'. qPCR was performed with the universal miRNA reverse primer 5'- CCAGTCTCAGGGTCCGAGGTATTC-3' and specific miRNA forward(F) primer. U6-snRNA was used for normalization. Primer sequences are listed in the Table S7.

Gene set enrichment analysis (GSEA)

GSEA was performed by using the *fgsea* function in the *fgsea* R package[70] on cell type signature gene sets from the Molecular Signatures Database (MSigDB).[30,31] Directional *fgsea* statistical enrichment tests were conducted. The genes were ranked by shrunk $\log_2$(FoldChange) computed by using the *lfcShrink* function in the *Deseq2* package.[68] The Shrinkage estimator *ashr* was used for the computation of shrunk $\log_2$(FoldChange).[71]

Quantitative RT-PCR

cDNA libraries from 1 μg of DNase I-treated total RNA were generated using the High-Capacity cDNA Reverse Transcription Kit (Applied Biosystems). qPCR was conducted in triplicates (6.2 μl/reaction) with 0.2 μM of primers and Maxima SYBR Green/ROX qPCR Master Mix (2X) (Thermofisher Scientific), on 7900HT Fast Real-Time PCR System (Applied Biosystems). Relative gene expression was calculated by $2^{-\Delta CT}$ method, where threshold cycle (CT) values of target genes were normalized to *Gapdh* gene.

DNA isolation

Cells were incubated in DNA lysis buffer (200 mM NaCl, 100 mM Tris pH 8.0, 10 mM EDTA, 0.5% SDS, Proteinase K 0.2 ug/mL) overnight at 55°C. Following 10 min of heat inactivation at 70°C, samples were treated with RNase A (0.2 ug/mL) at 37°C for 30 min. Lysates were then sonicated thrice on UCD-200 Bioruptor (low power, 30 seconds ON and 70 seconds OFF). DNA was extracted by phenol-chloroform and ethanol precipitation.

Molecular cloning

Plasmid containing *ApoE3* coding sequence (CDS, OHu27296) was purchased from GenScript. *ApoE4* CDS was amplified with *APOE4_mut_F* and *APOE4_mut_R* primers using Phusion High-Fidelity DNA Polymerase kit (NEB). ZymoTaq DNA Polymerase (Zymo Research) and PrimeSTAR Max (Takara Bio) was used to subclone *ApoE3* and *ApoE4* CDS into the *XbaI/SalI* restriction sites of the *pLVX-C-term-Flag-IRES-puro* lentiviral vector. Primer pairs *5XbaI_APOEXATG_Cterm* and *3SaI_APOEXATG_Cterm* that removed Kozak sequence and start codon from *ApoE3* were used to subclone *APOExStart* into *pLVX-C-term-Flag-IRES-puro* lentiviral vector. Primer pairs *5XbaI_APOEXATG_Cterm/APOE_3SalI_199a5p_1R* and *APOE_5XbaI_199a5p_2F/3SaI_APOEXATG_Cterm* were used to subclone the *APOExStart* N-terminal sequence and C-terminal sequence respectively into *pLVX-C-term-Flag-IRES-puro* lentiviral vector. Primer sequences are listed in the Table S7.

Transient transfection and lentiviral transduction

The Lenti-X lentiviral expression system (Clontech) was used to generate stable NSC lines that expressed either APOE3 or APOE4 C-terminal Flag-tag proteins. Briefly, lentivirus was prepared by transfecting 293T cells with a mixture that include Lenti-X packaging single shot reagent (VSV-G) (Clontech, 631275) and lentiviral vector (either *pLVX-APOE3-C-term-Flag-IRES-puro*, *pLVX-APOE4-C-term-Flag-IRES-puro*, or *pLVX-APOE3xStart-C-term-Flag-IRES-puro*). Media harvested at 24 h and 48 h post-transfection was combined with Lenti-X concentrator (Clontech, 631231). After overnight incubation and centrifugation, lentiviral supernatant was obtained by resuspending the pellet. NSC were infected with lentiviral supernatant in the presence of polybrene (12 μg/ml). After 48 h of viral transduction, stable clones were selected with 0.1 μg/ml of puromycin. Expression of stable NSC lines that contained either APOE3 or APOE4 were validated using qRT-PCR and western blot.

Immunofluorescence/EdU measurement of cell proliferation in cell culture

Neurons cultured in 12-well plates were fixed with 4% paraformaldehyde in 1× PBS for 20 min at room temperature and gently washed twice with 1× PBS. Neurons were incubated with blocking buffer (10% normal goat serum, 0.1% Triton-X 100 in 1× PBS) for 1 h at room temperature. This was followed by overnight incubation with specific primary antibodies in the blocking buffer at 4°C. After three gentle 1× PBS washes, neurons were incubated with secondary antibodies in blocking buffer for 1-2 h at room temperature. Following three 1× PBS washes, neurons were mounted in VECTASHIELD with DAPI (Vector Labs).

To measure EdU incorporation, neurons were incubated with 10 μM of EdU in the neuronal maturation medium 24 hours prior to fixation. Following two washes with 3% w/v BSA in 1× PBS, the neurons were permeabilized in 0.5% Triton-X 100 in 1× PBS for 20 min at room temperature and washed twice with 3% w/v BSA in 1× PBS. The EdU reaction cocktail from the Click-iT EdU Cell Proliferation Kit for Imaging (Thermo Scientific) was setup according to the manufacturer's instruction and added to the neurons (300 μL/well). Following 30 min of incubation in the dark and one round of wash with 3% w/v BSA in 1× PBS, the neurons were subjected to antibody staining protocol as described above.

Images captured with either Olympus (IX71, 20× objective) or confocal microscopes (FV3000, 10× objective) were analysed using Imaris software (version 9.2.0, Bitplane). A minimum of six fields were captured for each condition. For quantification, the signal threshold was adjusted to obtain optimal coverage of MAP2 positive soma and neurites of the neurons. The number of DAPI and/or EdU-stained nuclei was counted. Relative MAP2 density was calculated by dividing MAP2-positive area over the number of nuclei whereas H3K27me3 level was determined by dividing H3K27me3 signal intensity over its total area. The statistical significance was tabulated using the relative density/level of all the fields from each condition.

Prediction of secondary RNA duplex structure

Secondary structures of putative RNA duplex between *miR-199a-5p* and *ApoE* CDS were generated using the "Predict a Bimolecular Secondary Structure" module from RNAstructure web servers with DuplexFold algorithm on default settings.[72] A maximum of 32 bases from *ApoE* CDS were used to query either *hsa-miR-199a-5p* or *hsa-miR-618-5p* (as negative control). Potential miRNA target sites in the *ApoE* CDS were selected based on its complementarity to the 5'-seed sequence (position 2 to 7) of miRNAs and summarized in Table S6.

QUANTIFICATION AND STATISTICAL ANALYSIS

Quantitative PCR/ROS data are presented as mean ± S.D. of triplicate qPCR reactions/relative ROS readings and compared using unpaired 2-tailed student's *t*-tests unless otherwise stated in figure legends.

Immunoblot quantification data are presented as mean ± S.E.M or S.D. and compared using paired 2-tailed student's *t*-tests unless otherwise stated in figure legends. Immunofluorescence image quantification data are presented as mean of five or more microscopy images ± S.D. and compared using 2-tailed student's *t*-tests unless otherwise stated in figure legends. Statistical analysis for the student's *t*-tests was performed using Microsoft Excel.

The GSEA charts were generated by plotting the top gene sets with the highest -$\log_{10}$(adjusted *p*-value) from the directional GSEA test using the *fgsea* package in R. The cell type specific gene sets from MSigDB were used for the analysis. GO term analyses cut-offs are marked in red in Table S2.